DTI Tractography for Neurosurgical Planning: A Grand Challenge

Sunday September 18, 2011

MICCAI 2011, Toronto, Canada

Sonia Pujol, Ph.D.
Surgical Planning Laboratory, Brigham and Women's Hospital, Harvard Medical School

Ron Kikinis, M.D.
Surgical Planning Laboratory, Brigham and Women's Hospital, Harvard Medical School

Alexandra Golby, M.D.
Department of Neurosurgery, Brigham and Women's Hospital, Harvard Medical School

Guido Gerig, Ph.D.
The Scientific Computing and Imaging Institute, University of Utah

Martin Styner, Ph.D.
Neuro Image Research and Analysis Laboratory, University of North Carolina

William Wells, Ph.D.
Surgical Planning Laboratory, Brigham and Women's Hospital, Harvard Medical School

Carl-Fredrik Westin, Ph.D.
Laboratory of Mathematics in Imaging, Brigham and Women's Hospital, Harvard Medical School

Sylvain Gouttard, M.Sc.
The Scientific Computing and Imaging Institute, University of Utah

Table of Contents

Involving machine learning and particule mass in the segmentation of cortico-spinal tract

Caroline C. Brun[1], Hongzhi Wang[1], Ramón Aranda[2], Alonso
Ramìrez-Manzanares[3], Mariano Rivera[2], Paul A. Yushkevich[1], James C. Gee.[1]

[1] Penn Image Computing and Science Laboratory, University of Pennsylvania,
Philadelphia, PA, 19104, USA
[2] Centro de Investigación en Matemáticas, Guanajuato, Gto, México, 36240
[3] Universidad de Guanajuato, Departemento de Matemáticas, Guanajuato, Gto,
México, 36240

Abstract. In this paper, we take full advantage of the information contained in diffusion-weighted images (DWI) to extract a major brain white matter bundle, the cortico-spinal tract (CST). The gist of the method is to combine cutting-edge machine learning, registration and tractography techniques into an automatic pipeline that takes the DWI as an only input, independently of the subject's neurological condition, and model the cortico-spinal tracts based on robust prior-assumptions. This tool is however flexible as disease-specific information can be added on if appropriate. For a given subject's set of DWIs, the DTI is reconstructed, registered to an existing adult DT atlas using a piecewise-affine DT-based registration algorithm. Existing regions of interest (ROIs) defining the CSTs are propagated from the atlas space to the subject space. They are then corrected using a learning-based wrapper adapted to our problem. The fiber bundle is then extracted using an efficient tractography method, based on stochastic walk of particules with mass.

1 Introduction

Defining the location of given white matter bundles remains a very challenging task, in particular in the context of neurosurgery operating rooms where efficiency has to be combined with the greatest possible precision. In fact, each image specific, such as poor SNR or unusual neurological conditions, can hamper the proper segmentation of well-known major white matter tracts. Tools are being developed to address this problem of utmost importance and make such segmentations more efficient and accurate [6].

White matter tract segmentation can be categorized into two groups. The first one encompasses methods that consist of a deterministic ([8], [11]) or probabilistic ([15], [4], [9]) tractography of the whole brain, followed by an independent filtering of the tracts through regions of interests determined by the user in meaningful anatomical regions [17]. This approach was chosen to generate tract-specific analyses in [19], for instance. This type of method heavily depends on the quality of the whole brain tractography as well as on the anatomical accuracy of the inclusion and exclusion ROIs. A second class tackles this problem

by targeting a given bundle, which is the case in Kreher et al. [7], where the authors rely on probabilistic maps obtained from two seed points to delineate white matter structures. In addition, in [21], a gaussian-based inner product is computed between fibers, and used for automatic tracts bundling.

Motivated by the work from Nazem-Zadeh et al. [13], in this paper, we pipeline innovative DTI-based registration, machine learning and tractography algorithms to segment the corticospinal tract, a voluntary movement motor tract, of 2 patients with tumor and 2 healthy subjects with 10 repeated scans provided by the organizers of the DTI challenge workshop. After preprocessing of the DWIs, Diffusion Tensor Images were reconstructed. The 10 repetitions of the healthy subjects's DTIs were averaged using a piece-wise affine registration algorithm[18]. These averages and the patient's DTIs were then registered to an existing adult DTI atlas [5] built from the publicly available IXI database. The ROIs defined on this atlas were then propagated to each subject. The propagated ROIs for each subject were further refined by applying a learning-based wrapper method [20] that aims at reducing systematic label errors with respect to manually delineated ROIs. The last step was to use these corrected ROI to filter the whole brain tractography obtained with a robust algorithm based on stochastic walks of massive particles [1]. This algorithm allows to accurately recover estimates of the axon bundle orientations at fiber crossings, using a multi diffusion tensor field computed from the means of the Diffusion Basis Function model [14].

2 Method

2.1 Presentation of the analysis pipeline

Normalizing the Diffusion images to an existing atlas For all 22 sets of images (two patients and two times 10 subjects's scans), all the gradient acquisitions were affinely aligned to the b_0 image to correct for motion and a whole brain mask was created using Brain Extraction Tool ([16]). The b_0 aligned weighted-images and brain mask served as inputs for the Diffusion Tensor reconstruction achieved with the Diffusion Tensor Image Toolkit (DTI-TK, dti-tk.sourceforge.net). Irregularities, such as non definite positive tensors were corrected for and the DTIs were linearly and nonlinearly registered to a DT adult atlas, using a high-dimensional tensor-based image registration algorithm [18]. The DT adult atlas was built from 78 images drawn from the 550 healthy subject scans of the IXI database (40 males/38 females- ages: 39.77 ± 11.63 / 39.47 ± 12.51) [5] and was chosen over an aging population template, after visual inspection of the scans to analyze. The tumor segmentations provided by the organizers of the workshop were also propagated from the T_1 and T_2 weighted structural images to the DTIs, using a symmetric diffeomorphic mapping contained in the Advanced Normalization tool (ANTS) [2]. The Fractional anisotropy and mean diffusivity images derived from the DTIs were registered to the T_1 and T_2, respectively. The inverse of the displacement fields were applied to the tumor segmentation. Visual inspection of the segmentation overlayed on top of principal

direction and fractional anisotropy images allows us to classify each segmentation into 3 categories: edema, infiltrated or disrupted areas. The segmentation corresponding to the disrupted tumored areas were added as exclusion criteria while filtering the CST from the whole brain tractography.

Definition and Refinement of the ROIs

- *Definition of the ROIs:* Regions of interest, called *inclusion ROIs* (i.e., ROIs through which the CST goes) were manually defined by a specialist on the FA-weighted principal direction images of the adult atlas and 10 other randomly chosen IXI subjects in their original space (Figure 1). They were selected in agreement with the ICBM-DTI-81 white matter probabilistic atlas [12]. As the CST is an ascending tract, these inclusion ROIs were delineated on axial slices at the pons level and at the junction between the temporal lobes and the somatosensory cortex in each hemisphere. A mid-sagittal *separation plane* was also traced that served as an exclusion ROIs. All the ROIs were then propagated from the atlas space to each subject space (see Figure 1). Disrupted tumored areas flowed from the subject's structural to the subject's DT space also represented exclusion ROIs in patients.

- *Automatic segmentation:* The atlas ROIs were propagated from the normalized space to each control, patient and IXI images' space using the inverse deformation field obtained from prior registration of the DT images to the atlas. They were further propagated in the case of the controls to match each of the 10 repeated scans.

- *Learning phase:* The refinement or learning phase is crucial to improve the accuracy of the propagated ROIs, hence the accuracy of the segmentation accuracy. We did so by adapting the corrective learning technique [20] that trains classifiers to identify and correct systematic errors between the automatic ROIs and the expert labeled ROIs. To this end, the ROIs drawn in each of the IXI original space was taken as a ground truth and compared to the automatic segmentation obtained for each of these subjects. Comparing to classical learning-based segmentation techniques, the key advantage of corrective learning is that it allows the learning algorithm to efficiently incorporate the anatomical context information of the CST encoded via atlas propagation, such as the direction of the fiber bundle in different regions of the brain, to improve the learning performance.

Tractography of the CST To estimate axonal fiber connectivity pathways on the CST, we used the algorithm proposed in [1], based on stochastic walks of massive particles. The method relies on multiple local orientation information provided by multi tensor diffusion MRI to lead the particles. It uses particles with mass, which introduces inertia and gravitational forces resulting in filtered trajectories. Following this, the fiber bundles are estimated

with a clustering procedure based on terminal points (the tractography positions on the ends of the tracto which are expected to reach white-grey matter interfaces) that allows to eliminate outlier walks generated by wrong seed points or wrong trajectories. We also filter the tracts that reach target ROIs. These ROIs are introduced to the tractography stage so that a correct walk must start from one region and end on the other. To define those ending regions we use the inferior and superior inclusion corrected ROIs we defined in the previous stage.

The vector $x_{t,m}$ defines the position of the m-th particle at the iteration (step) t. $x_{t+1,m} = x_{t,m} + \alpha d_{t+1,m}$ is the new position of the m-th particle, where the motion direction is denoted by the unitary vector $d_{t+1,m}$ and α is a fixed step size. In this approach, the motion direction is given by $d_{t+1,m} = \gamma_1 d^1_{t+1,m} + \gamma_2 d^2_{t+1,m} + \gamma_3 d^3_{t+1,m}$. The first term codifies the information of the local fiber orientation and is stochastically selected from the principal direction diffusions of the multi-tensor representation. The second term introduces an inertial component into the particle's trajectory, and the last term introduces gravitational effect of the surrounding particles promoting similar trajectories to the entire particle set. The most important component of the particle's dynamic is the first term $d^1_{t+1,m}$, *i.e.* the local tissue structure.

2.2 Description of the parameter used in each of the algorithms

DTI and structural normalization Two registration algorithms were used to a/ normalize all the diffusion tensor images to the IXI atlas and to b/ normalize the T_1 and T_2 structural images to the DTIs. In the first case, the DWIs were all preprocessed in the same way. In fact, they initially had various origins: the number of diffusion-weighted images were different for the patients, the controls and the IXI subjects. These datasets were also acquired on different scanners, with different resolutions and voxel spaces. In order to minimize the bias resulting from this diversity, we used algorithms that have been thoroughly tested and shown to be extremely robust. In addition, diffusion tensors images are the only images from which comparisons (i.e., registrations) are inferred. DTs model the real diffusion signal while approximating it, and thus are less subjected to bias. The DWIs were corrected for motion and eddy-current artifacts ([10]), before extracting the brain from the b_0 image using BET ([16]). The threshold for the extraction was set to 0.2. Each subject's DT was then reconstructed using the standard linear regression approach [3], and resampled to 256x256x256 voxels with dimensions equal to 1x1x1mm.

These resampled DTIs were first rigidly and affinely aligned to the template using the Euclidean Distance squared as a similarity metric, $x = 4$ mm, $y = 4$ mm and $z = 4$ mm, as the distance between the sample points to evaluate image similarity. The stop criterion was $\delta = 0.01$ (minimum amount of change in the cost function as a fraction of the previous

value at the previous iteration). These linearly registered DTIs were inputted into a diffeomorphic registration algorithm. This one uses the L^2 distance between the anisotropic part of the apparent diffusion profiles associated with the DTs as a similarity metric and, regularizes the transformation using a dense piecewise affine parametrization, which divides the template space into uniform regions and parametrizes the transformation within each region by an affine transformation. The DTs are explicitly reoriented at each step using the finite strain method [18]. As recommended here http://dti-tk.sourceforge.net/pmwiki/pmwiki.php?n=Documentation.Registration, we used 6 iterations and a stopping criterion equal to 0.002.

A second step consisted of aligning the T_1 and T_2 to the fractional anisotropy (FA) and mean diffusivity (MD) images for each patient and apply this transformation to the tumor segmentations. We used the a symmetric diffeomorphic normalization (SyN) [2], with a 3-level multiresolution scheme and cross-correlation as a similarity metric. In both case, the radius kernel was 3 voxels, the gradient descent step size 0.1 and the gaussian smoothing with a σ of 0.25.

Machine Learning correction Note that each inclusion ROI is defined in a single axial slice. Before propagation, the ROI was dilated over 2 voxels in the direction orthogonal to its surface, which is possible because the ROIs would be similar in neighboring slices. This was done to ensure that the ROI resulting from the propagation would not present any irregularities due to interpolation during registration.

After transportation from the atlas to the target image, each propagated inclusion ROI may span over more than one axial slices. Thus, for training we projected the propagated ROI into the corresponding axial slice where the ROI was manually delineated. This projected ROI was used as the initial automatic ROI segmentation, upon which the corrective learning was applied to make improvement. We applied corrective learning to each inclusion ROI separately. For testing, as the axial slice containing the manually delineated inclusion ROI is unknown, we estimated the axial slice for each inclusion ROI by computing the mass of center of the automatically propagated ROI. The atlas-propagated ROI was then projected into the estimated axial slice. The projected ROI was used as the initial ROI segmentation and the correction was performed within the estimated axial slice. Note that for the mid-sagittal separation ROI, corrective learning is unnecessary. The location of this ROI was estimated by computing the mass center of the propagated separation slice.

For the corrective learning step, we defined the *correction ROI* by performing a one-voxel dilation operation within the axial slice to the set of all voxels labeled as an inclusion ROI in the initial automatic ROI segmentation. We trained an AdaBoost classifier to identify the inclusion ROI voxels labeled by a human expert only within the correction ROI. The use of the correction ROI was motivated by the fact that when the host method works reasonably

well, most voxels labeled as the inclusion ROI in the initial segmentation are in the close proximity of the inclusion ROI voxels in the manual segmentation. Defining correction ROI simplifies the learning problem by excluding the vast majority of irrelevant background voxels from consideration.

We adapted the features used in [20] for structural MRI to train the AdaBoost classifiers for the DTI data. In summary, the features captured the FA together with the information on principal directions extracted from the reconstructed DTI and contextual information captured in the initial inclusion ROI segmentation for each voxel. The contextual features $L(i)$ were extracted from the automatic ROI segmentation, S, with $L^{\Delta x, \Delta y, \Delta z}(i) = S(x_i + \Delta x, y_i + \Delta y, z_i + \Delta z)$. (x_i, y_i, z_i) is the coordinate of voxel i and $(\Delta x, \Delta y, \Delta z)$ is the relative location from it. Similarly, the features extracted from FA and weighted rgb-images are represented as $F^{\Delta x, \Delta y, \Delta z}(i) = F_A(x_i + \Delta x, y_i + \Delta y, z_i + \Delta z)$ and $R^{\Delta x, \Delta y, \Delta z}(i) = I_{red}(x_i + \Delta x, y_i + \Delta y, z_i + \Delta z)$, $G^{\Delta x, \Delta y, \Delta z}(i) = I_{green}(x_i + \Delta x, y_i + \Delta y, z_i + \Delta z)$, $B^{\Delta x, \Delta y, \Delta z}(i) = I_{blue}(x_i + \Delta x, y_i + \Delta y, z_i + \Delta z)$, respectively, where F_A is the FA image and $I_{\{.\}}$ are the weighted rgb-images representing the principle directions. In our experiment, these features were sampled in a $5 \times 5 \times 5$ neighborhood of a given voxel (i.e., $\Delta x, \Delta y, \Delta z \in [-2, 2]$). In addition, the normalized spatial coordinates of each voxel $S_x(i) = x_i - \overline{x}$, $S_y(i) = y_i - \overline{y}$, where $\overline{x}, \overline{y}$ are the coordinates of the center of mass of the correction ROI in the axial slice, and the joint feature obtained by multiplying each spatial feature and each contextual, FA and R, G, B features, as used in [20], were included as well.

After the training step, we applied the classifiers learnt from the IXI database to improve the segmentation accuracy of the automatically generated ROIs on controls and patients. To further refine the corrected ROI, we applied an anatomical prior that each inclusion ROI voxel should have the following property $I_{blue} > 80$, $I_{blue} > I_{red}$ and $I_{blue} > I_{green}$. The CST is in fact an ascending tract, which fans out as reaches the gray matter boundary. Thus, the blue channel corresponding to the principal direction inferior-superior must be greater than the two other intensities. The value 80 indicates a high FA value. The resulted ROI segmentation may contain multiple isolated regions. The largest connected component was selected to be the final inclusion ROI segmentation.

Probabilistic Tractography A small fixed step size $\alpha = 0.4$ was set, which promotes a careful analysis of the regions with fiber crossings and bifurcations. $\gamma_i's$ values were set to 0.7, $1 - \gamma_1$ and 1, respectively. The gravitational force between particle was 0.00001, this value promotes the correction of the particles' trajectories as well as a thorough exploration of the medium (where bifurcations occurs). A particle was stopped when it reached a voxel with FA value lower than 0.2. The global stop criterion was reached when all the particles' walks were stopped. We clustered the fibers pathways and discarded the pathway outliers as is explained in the following. Each pathway has an initial point, a

trajectory and an ending point, and the most important feature for clustering the pathways are their final position. The cluster stage is based on the single linkage distance between clusters, also called nearest neighbors. Single linkage uses the smallest distance between objects in two clusters, c_1 and c_2. Thus if $d(c_1, c_2) < c$, (where $d(\cdot, \cdot)$ is the Euclidean distance) c_1 and c_2 are joined. Once the clusters are computed, clusters with only a few fibers are eliminated. Finally, we set $c = 2$ and $\varphi = 0.01$.

3 Results

The increased accuracy obtained from the learning technique was assessed in table 1. Manual segmentations of the 4 ROIs needed to isolate the CST were drawn in patient 1's FA-weighted image. Dice coefficients were computed to compare the automatic segmentation to the corrected one. The correction step noticeably improved the result, except for the tumor region as the prior information used in the learning phase did not account for the loss of FA. However, in the case of patient 1, the specificity is achieved by using the segmentation of the disrupted tumor as an exclusion ROI when the CST is filtered out of the whole brain tractography. Figure 2 shows the resulting segmentations for one of the patients and one of the subjects. On the right panel, the left CST was displaced because of the presence of the tumor. The segmentation obtained for the healthy subject shows that the pipeline recovered the fan-like shape of the CST in the absence of tumor, even with a poor SNR. Figure 3 compare the segmentations obtained with and without the corrective algorithm. Using the propagating ROIs results in a sensible segmentation. However, the propagation generates a bias, in that it may extend the ROIs to areas that are not relevant to the CST, hence the addition of tract that do not belong to the given tract.

4 Conclusion

This method, solely based on diffusion-weighted images, was designed to automatically and efficiently segment the cortico-spinal tract, using cutting-edge algorithms in the field of registration, tractography and machine learning. However, the results obtained with this approach could be improved in several ways. As the resolution of the subjects's scans were poor, we could have taken advantage of the ten repeated scans, by normalizing all the diffusion weighted images to the same space, and consider the whole set of 250 diffusion weighted images for the reconstruction of the DT and the tractography. Even so, our aim was to challenge our algorithm using low-SNR sets of DWI, as can be the case in operating rooms. Repeating the CST segmentation on 10 repetitions can serve to validate the consistency and robustness of a given technique. Another improvement to our pipeline would be to add more subjects to our training data. In fact, in this paper, we used a DTI dataset from heatlhy subjects to correct segmentations for patients

and controls. Other training images could be included, such as patients with different type of tumors. A constrain could then be added to the training in order to correct initial segmentation with this information.

5 Appendix: Proposed evaluation criterion

To quantitatively evaluate the accuracy of the automatically produced CST tractography, we propose a high level criterion adapted from the criterion used in segmentation evaluation.

First, a gold standard CST region within each hemisphere is delineated by a human expert for each testing subject. For the evaluation, each automatically produced CST tractography within each hemisphere is converted into a binary envelope segmentation. The envelope CST segmentation can be derived by applying spatial smoothing on the produced CST tracts. The agreement between the automatically produced CST segmentation and manually delineated CST region defines an objective measurement showing the accuracy of the CST tractography.

The advantage of this evaluation approach is that it is based on high level, global shape information, which can be objectively implemented with moderate human effort. The key limitation of this evaluation approach is that it does not reflect any low level, detailed evaluation for each individual tract.

References

1. Aranda, R., Rivera, M., Ramìrez-Manzanares, A., Ashtari, M., and Gee, J.C., *Massive Particles for Brain Tractography*, Lecture Notes in Computer Science, 6437, p 446–457, (2010)
2. Avants, B. B., Epstein, C. L., Grossman, M., Gee, J. C., *Symmetric diffeomorphic image registration with cross-correlation: Evaluating automated labeling of elderly and neurodegenerative brain*, Med Image Anal, 12, 26–41, (2008)
3. Basser, P.J., Mattiello, J., Le Bihan, D., *Estimation of the effective self-diffusion tensor from the NMR spin echo*, J. Magn. Reson., 103, p 247–254, (1994)
4. Bergmann, O., Kindlmann, G., Peled, S., Westin, C.F. *Two-tensor fiber tractography*, IEEE ISBI, Washington, D.C., (2007)
5. Brun, C.C, Zhang, H., Yushkevich, P.A, Rueckert, D., Gee, J.C., *Exploring gender differences in white matter using a new tract specific atlas*, OHBM, Québec, Canada, (2011)
6. Golby, A.J., Kindlmann, G., Norton, I., Yarmarkovich, A., Pieper, S., Kikinis, R., *Interactive diffusion tensor tractography visualization for neurosurgical planning*, Neurosurgery, 68(2) p 496–505, (2011)
7. Kreher, B.W., Schnell, S., Mader, I., Ilyasov, K.A., Hennig, J., Kiselev, V.G., Saur, D., *Connecting and merging fibres: Pathway extraction by combining probability maps*, NeuroImage 43, 81–89, (2008)
8. Lenglet, C., Deriche, R., Faugeras, O., *Diffusion tensor magnetic resonance imaging: Brain connectivity mapping*, Research Report 4983, INRIA (2003)
9. Malcolm, J.G., Michailovich, O., Bouix, S., Westin, C.F., Shenton, M.E., Rathi, Y.,*A filtered approach to neural tractography using the watson directional function*, Medical Image Analysis 14, p 58–69 (2010)

10. Mangin, J.F., Poupon, C., Clark, C. A. , Le Bihan, D., Bloch, I., *Distortion correction and robust tensor estimation for MR diffusiong imaging*, Med. Image Anal., 8, p 191–198, (2002)

11. Mori, S., Xue, R., Crain, B., Solaiyappan, M., Chacko, V.P., van Zijl, P.C.M.,*A filtered approach to neural tractography using the watson directional function*, ISMRM, (1999)

12. Mori, S., Oishi, K., Jiang, H., Jiang, L., Li, X., Akhter, K., Hua, K., Faria, A.V., Mahmood, A., Woods, R., Toga, A.W., Pike, G.B., Neto, P.R., Evans, A., Zhang, J., Huang, H., Miller, M.I., van Zijl, P., Mazziotta, J. *Stereotaxic white matter atlas based on diffusion tensor imaging in an ICBM template*, NeuroImage (40), p 570–582, (2008)

13. Nazem-Zadeha, M.-R., Davoodi-Bojda, E., and Soltanian-Zadeh, H., *Atlas-based fiber bundle segmentation using principal diffusion directions and spherical harmonic coefficients*, NeuroImage, 54(1), p 146–164, (2011)

14. Ramirez-Manzanares, A., Rivera, M., Vemuri, B.C., Carney, P., Mareci, T., *Diffusion Basis Functions Decomposition for Estimating White Matter Intravoxel Fiber Geometry*, IEEE Trans. Med. Imaging., 26, p 1091–1102, (2007)

15. Savadjiev, P., Rathi, Y., Malcolm, J.G., Shenton, M.E., Westin, C.F., *A geometry-based particle filtering approach to white matter tractography*, MICCAI, Beijing, China, Part II, p 233–240, (2010)

16. Smith, S.M., *Fast robust automated brain extraction*, Human Brain Mapping, 17, p 143–155, (2002)

17. Wakana, S., Jiang, H., Nagae-Poetscher, L.M., van Zijl, P.C., Mori, S., *Fiber tract-based atlas of human white matter anatomy*, Radiology, 230, 77–87 (2004)

18. Zhang, H., Yushkevich, P., Alexander, D., Gee, J., *Deformable registration of diffusion tensor MR images with explicit orientation optimization*, Med Image Anal, 10(5), 764–785 (2006) Hui Zhang*, Brian B. Avants, Paul A. Yushkevich, John H. Woo, Sumei Wang, Leo F. McCluskey, Lauren B. Elman, Elias R. Melhem, and James C. Gee

19. Zhang, H., Awate, S.P., Das, S.R., Woo, J.H., Melhem, E.R., Gee, J.C., and Yushkevich, P.A., *A Tract-Specific Framework for White Matter Morphometry Combining Macroscopic and Microscopic Tract Features*, MICCAI, London, Part II, p. 141–149, (2009)

20. Wang, H., Das, S.R., Suh, J.W., Altinaya, M., Pluta, J., Craige, C., Avants, B, Yushkevich, P.A., and the Alzheimers Disease Neuroimaging Initiative, *A Learning-Based Wrapper Method to Correct Systematic Errors in Automatic Image Segmentation: Consistently Improved Performance in Hippocampus, Cortex and Brain Segmentation*, NeuroImage, 55(3), p 968–85 (2011)

21. Wassermann, D., Bloy, L., Kanterakis, E., Verma, R., Deriche, R., *Unsupervised white matter fiber clustering and tract probability map generation: applications of a Gaussian process framework for white matter fibers*, NeuroImage, 51(1), p 228–241 (2010)

Segmentation	Label (Fig. 1)	Automatic	Corrected
Left Inferior	green	0.419	0.687
Right inferior	red	0.339	0.785
Left Superior	blue	0.811	0.826
Right Superior	yellow	0.819	0.880

Table 1. Comparison between automatic and corrected segmentations in patient 1, displayed for the 4 ROIs used to filter the CST bundle. The manual segmentation is taken as the reference. The correction noticeably improved the result, except for the tumor region as the prior information used in the learning phase did not account for the loss of FA
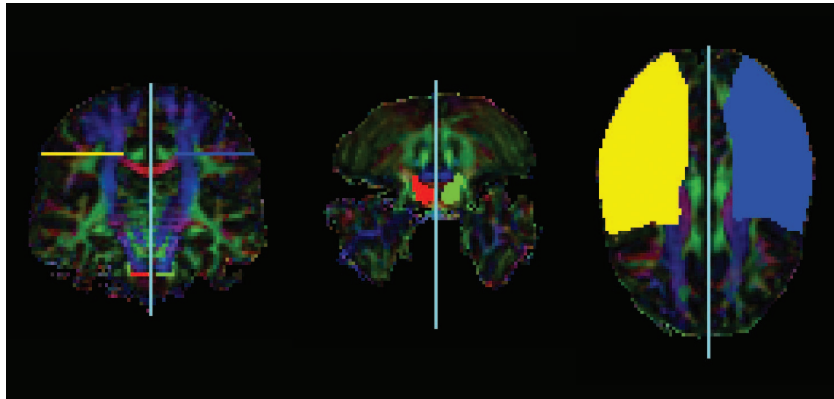

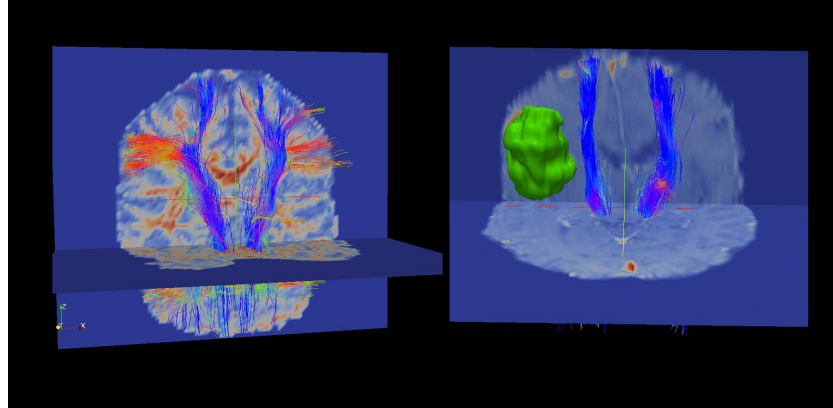**Fig. 1.** Illustration of the manually defined Regions of Interest on one of the subjects from the IXI database

Fig. 2. Left Panel: Segmentation of the left and right cortico-spinal tract superposed on top of the FA image. **Right Panel**: Segmentation of the left and right cortico-spinal tract in patient 1.
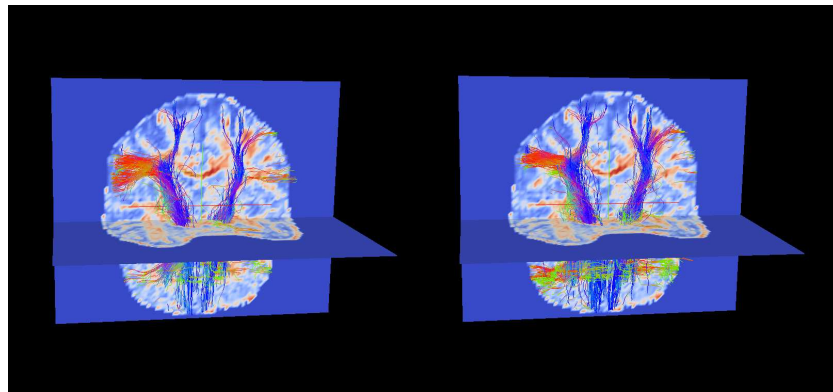

Fig. 3. Comparison of the right and left CST obtained with (left) and without (right) correction. Using the learning algorithm provides a means to refine the ROIs, hence to achieve more precise definitions of the tracts

Tractography in the CST using an Intrinsic Unscented Kalman Filter

Guang Cheng, Hesamoddin Salehian, and Baba C. Vemuri†⋆

CISE, University of Florida

1   Introduction

In this short paper, we present a *novel tractography* method based on *a generalization of unscented Kalman filter(UKF)* which involves the use of intrinsic geometry of the space of symmetric positive definite matrices denoted henceforth by P_n. Such a generalization has never been reported in literature to date. We call this new filter the intrinsic unscented Kalman filter (IUKF). In this filter, operations that are intrinsic to P_n are employed and thus no explicit constraints are needed to guarantee the positive definiteness of the estimated diffusion tensors unlike in [1]. This method is applied to the given human brain data to perform tractography and recover the CST.

2   Methods

Our tractography algorithm consists of three steps, namely, (1) preprocessing, (2) fiber tracking and (3) fiber reduction. We now describe each step in some detail.

(1) In the preprocessing step, each volume corresponding to a given magnetic gradient direction from the DW MRI dataset is denoised using the unbiased non-local means algorithm for Rician noise [2]. Since our tracking method is based directly on the MR Signals, no multi-fiber reconstruction over the whole image lattice is needed as a preprocessing step. However, the DTI reconstruction method [3] is employed at the seed points as the initialization for the IUKF.

(2) In this fiber tracking stage, the IUKF is combined with a streamline algorithm, which is initialized from a seed point. Here all the seeds are uniformly distributed in a rectangular box that covers most of the brain. At iteration step k for a single fiber, the reconstruction is performed by the IUKF using a bi-tensor model, and the direction $\mathbf{d}_k$ is computed as the major eigen vector of one of the tensors that is closer to the direction from the last step. The streamline algorithm then updates the position by computing $\mathbf{x}_{k+1} = \mathbf{x}_k + \Delta t \mathbf{d}_k$, where Δt is the step size. The tracking stops if the angle between $\mathbf{d}_k$ and the fiber direction is large (exceeds a angle threshold Θ_m), or it is at the boundary of the dataset. The parameters values used in our experiments are is summarized in Table (2.1);

---

(3) To get the final result, we also need to remove the fibers that do not belong to the corticospinal tract. This is done by a fiber reduction criteria applied to the tracking results obtained from the fiber tracking step.

2.1 The Intrinsic Unscented Kalman Filter for Diffusion Tensors

In this section, we briefly present a novel intrinsic unscented Kalman filter to track diffusion tensors. It is well known that diffusion tensors lie in the space P_n and we refer the reader to [4,5] for an introduction to the mathematical properties of P_n. The IUKF has three main components, namely, an observation model, the state transition model and the filter. The IUKF is similar to the standard UKF [6] with the key difference being, some of the vector operations, e.g. the update of the posterior are replaced by the general linear (GL) group operation on P_n. Here we will limit our explanation to the observation and state transition model.

The observation model is based on the bi-tensor diffusion model.

$$S_k^{(n)} = S_0(e^{-b_n \mathbf{g}_n^t \mathbf{D}_k^{(1)} \mathbf{g}_n^t} + e^{-b_n \mathbf{g}_n^t \mathbf{D}_k^{(2)} \mathbf{g}_n^t}) + \mathbf{w_n} \tag{1}$$

where $\mathbf{g}_n$ denotes the direction of n-th magnetic gradient, and b_n is the corresponding b-value, and $S_k^{(n)}$ is the MR signal encountered at the k-th iteration along the n-th magnetic gradient field direction. $\mathbf{w_n}$ is the additive observation noise. The covariance matrix of the observation noise for all the magnetic gradients is a diagonal matrix denoted by $\mathbf{R}$.

For the state transition model on P_n, we propose the general linear (GL) group operation/action and the LogNormal distribution [7]. For the bi-tensor (sum of two Gaussians) model, the state transition model at step k is given by,

$$\begin{aligned}
\mathbf{D}_k^{(1)} &= (\mathbf{F}\mathbf{D}_{k-1}^{(1)}\mathbf{F}^t)^{1/2} Exp(\mathbf{v}_k^{(1)})(\mathbf{F}\mathbf{D}_{k-1}^{(1)}\mathbf{F}^t)^{1/2} \\
\mathbf{D}_k^{(2)} &= (\mathbf{F}\mathbf{D}_{k-1}^{(2)}\mathbf{F}^t)^{1/2} Exp(\mathbf{v}_k^{(2)})(\mathbf{F}\mathbf{D}_{k-1}^{(2)}\mathbf{F}^t)^{1/2}
\end{aligned} \tag{2}$$

where, $\mathbf{D}_k^{(1)}$, $\mathbf{D}_k^{(2)}$ are the two tensor states at step k, $\mathbf{F}$ is the state transition GL-based operation, $\mathbf{v_k^{(1)}}$ and $\mathbf{v_k^{(2)}}$ are the Gaussain distributed state transition noise for $\mathbf{D}_k^{(1)}$ and $\mathbf{D}_k^{(2)}$ in the tangent space at the identity $\mathbf{I}$. The covariance matrices of the state transitions are $\mathbf{Q}^{(1)}$ and $\mathbf{Q}^{(2)}$ respectively. Exp is the matrix exponential. The square root of in Eq. 2 is defined as $\mathbf{P}^{1/2} := \mathbf{g}$, such that $\mathbf{g}\mathbf{g}^T = P$, and $\mathbf{g}$ is symmetric.

In this work, the covariance matrix of the observation noise is set to be a scaled identity matrix $\mathbf{R} = r\mathbf{I}$. And so is the covariance matrix of the state transition model set to $\mathbf{Q_1} = q_1\mathbf{I}$, $\mathbf{Q_2} = q_2\mathbf{I}$. The initialization of the IUKF is also important. Here at each seed point, a diffusion tensor reconstruction method [3] is employed to initialize $\mathbf{D}_0^{(1)}$, and $\mathbf{D}_0^{(2)} = |\mathbf{D}_0^{(1)}|^{2/3}(\mathbf{D}_0^{(1)})^{-1}$. The state transition matrix F is set to the identity. All the parameters settings are depicted in table 2.1.

Subject	$\Delta t(mm)$	Θ_M	q_1	q_2	r	Θ_c
Patient	0.5	60°	0.1	0.1	0.05	20°
Control	0.25	60°	0.1	0.1	0.03	3°

Table 1. Parameter Table.

2.2 Fiber Reduction

To remove the fibers that do not belong to the corticospinal tract, we need a post-processing step that reduces the unwanted fibers. Two reduction criteria are used, based on ROI and angle of the fiber to the MR-slice direction.

Firstly, each fiber should pass through both of the two ROIs, one at the top of the brain, and the other in the brainstem, as shown in the upper left figure in Fig 3, which is also the ROI where we put the seed points as the initialization of our tracking method. In this way, the fiber length criteria is implicitly applied such that only long fibers starting from brainstem and ending in the cortex are retained. The ROI in the experiments is manually set using ITK-SNAP [8].

Secondly, there are some fibers that are not sufficiently vertical. Therefore, we also used an angle threshold criteria to remove them. In this way, each fiber which has an angle less than a threshold (Θ_c) to the X-Y plane, is discarded. The value of Θ_c in our experiment is depicted in the table 2.1.

In the tracking stage, the left and right corticospinal tracts are tracked jointly. To split them, the mid sagittal plane is manually selected, and the fibers with larger portion in the right of the plane are treated as right corticospinal tracts and vice versa. Any fiber that passes the mid sagittal plane is discarded.

Lastly, retained fibers are all long enough to connect the brainstem to the cortex, and also are vertical enough to be included in corticospinal tract.

3 Experimental Results

The fiber tracking results from the first patient are depicted in Fig. 3, where we observe that the shape of the fiber bundle looks satisfactory, since the CST fibers connect the brainstem to the cortex. Also, from the figure on the top right we can see that the fiber bundle along the side of the tumor is thinner (squished) as expected. The fiber bundle is displayed using MedINRIA [9].

4 Conclusion

By using the IUKF, we can track fibers even in noisy datasets such as the scans from the healthy subject. However, since it is as streamline based method, there are still limitations, such as, it can not handle the fanning issue very well. That is, the results obtained starting from a smaller and bigger side of the fanning are not equivalent. So in this work, we use both the cortex and the brain stem for seeding the tractography. And this ROI can also be used as the fiber reduction criteria to reduce the unwanted fibers. In this way, satisfactory results are obtained even when the ROI is not an accurate segmentation from the dataset.
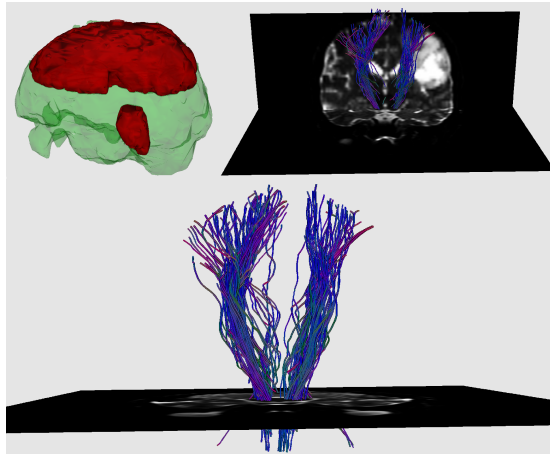
Fig. 1. Fiber reconstruction results for the first patient. The upper left figure is the ROI used as the seeds in the initialization of the fiber tracking and also the fiber reduction (region) criteria. The upper right figure overlays the fibers with two s0 image slices in the coronal and axial views, to depict the relative position w.r.t the tumor. The lower figure shows the shape of the fiber bundle.

References

1. James G. Malcolm, Martha Elizabeth Shenton, Y.R.: Two-tensor tractography using a constrained filter. In: MICCAI. (2009)
2. Wiest-Daessle, N., Prima, S., Coupe, P., Morrissey, S., Barillot, C.: Rician noise removal by non-local means filtering for low signal-to-noise ratio mri: applications to dt-mri. In: MICCAI. (2008)
3. Barmpoutis, A., Vemuri, B.C.: A unified framework for estimating diffusion tensors of any order with symmetric positive-definite constraints. In: ISBI. (2010)
4. Fletcher, P., Joshi, S.: Riemannian geometry for the statistical analysis of diffusion tensor data. Signal Processing **87** (2007) 250–262
5. Moakher, M.: A differential geometric approach to the geometric mean of symmetric positive-definite matrices. SIAM J. MATRIX ANAL. APPL. **26** (2005) 735–747
6. Wan, E., Van Der Merwe, R.: The unscented kalman filter for nonlinear estimation. In: AS-SPCC. (2000)
7. Schwartzman, A.: Random ellipsoids and false discovery rates: Statistics for diffusion tensor imaging data. PhD thesis, Stanford University (2006)
8. Yushkevich, P.A., Piven, J., Cody Hazlett, H., Gimpel Smith, R., Ho, S., Gee, J.C., Gerig, G.: User-guided 3D active contour segmentation of anatomical structures: Significantly improved efficiency and reliability. Neuroimage **31**(3) (2006) 1116–1128
9. Toussaint, N., Souplet, J.C., Fillard, P.: MedINRIA: Medical Image Navigation and Research Tool by INRIA. In: Proc. of MICCAI'07 Workshop on Interaction in medical image analysis and visualization. (2007)

Multifiber Deterministic Streamline Tractography of the Corticospinal Tract Based on a New Diffusion Model

Olivier Commowick[1], Aymeric Stamm[1], Romuald Seizeur[1,3], Patrick Pérez[4], Christian Barillot[1], Sylvain Prima[1], and Nicolas Wiest-Daesslé[1,2]

[1] VISAGES: INSERM U746 - CNRS UMR6074 - INRIA - Univ. of Rennes I, France
[2] Department of Neurology, CHU Rennes, France
[3] Department of Neurosurgery, CHU Brest, France
[4] Technicolor, Rennes, France
Contact: `Olivier.Commowick@irisa.fr`

Abstract. In this paper, we build upon a new model, describing the random motion of water molecules in fibrous tissues, to develop a multifiber deterministic tractography algorithm. We apply this algorithm to track the corticospinal tract of the human brain, in both controls and patients with tumors.

1 Introduction

Tractography of the corticospinal tract (CST) using diffusion-weighted MRI (DW-MRI) is especially challenging, mostly due to the numerous fiber crossings in the corona radiata. When classical diffusion models (e.g. single or multiple tensors) coupled with simple tractography algorithms (e.g. deterministic streamline) are used, these crossings often make it impossible to track the most lateral fibers of the CST [1]. These include especially important motor areas such as the hand and the whole face, as shown by the homunculus of Penfield & Rasmussen. The fact that HARDI sequences are prohibitively time-consuming in case of patients with tumors makes it critically important to develop diffusion models and/or tractography algorithms able to track these lateral fibers from clinical (fast) diffusion sequences, having a small number of encoding gradients. We recently proposed a diffusion model that seems to meet these requirements even when using a simple deterministic streamline algorithm [2].

We briefly outline this new model in Section 2.1, the tractography algorithm in Section 2.2, and the pipeline we used to extract the CST in Section 2.3. Finally, we provide tractography results of the left and right CST on the two controls and two patients of the challenge dataset in Section 3.

2 Methods

2.1 Diffusion Modeling

In each voxel, water molecules are assumed to be distributed in several compartments. We first describe how we model the diffusion within a single compartment.

Then, we introduce our multi-compartment model, coined Diffusion Directions Imaging (DDI), and finally we outline how to estimate its parameters.

Single-compartment Model The diffusion process induces, after a diffusion time τ, a random displacement of water molecules from their initial position $\boldsymbol{x}_0$ to a random position $\boldsymbol{x} = \boldsymbol{x}_0 + \sqrt{2\tau}\boldsymbol{w}$. Assuming a **unique** direction of diffusion, we propose to model the random variable $\boldsymbol{w}$ as $\boldsymbol{w} = \boldsymbol{u} + \boldsymbol{v}$, where:

- $\boldsymbol{u}$ follows a **von Mises & Fisher** distribution parametrized by (i) the radius $R > 0$ of the sphere on which it is defined, (ii) the spherical coordinates (θ, ϕ) of its mean direction $\boldsymbol{\mu}$ and (iii) its concentration parameter $\kappa \geq 0$;
- $\boldsymbol{v}$ follows a **centered Gaussian** distribution parametrized by a cylindrically constrained [3] covariance matrix $D = \frac{R^2}{\kappa+1}\left(I + \kappa\boldsymbol{\mu}\boldsymbol{\mu}'\right)$, where I is the identity matrix and $\{\boldsymbol{\mu}, \kappa, R\}$ are the same parameters that characterize $\boldsymbol{u}$;
- $\boldsymbol{u}$ and $\boldsymbol{v}$ are statistically independent.

In essence, (i) $\boldsymbol{\mu}$ can be interpreted as the direction of the fibers which constrain the diffusion, (ii) R can be interpreted as the radial displacement along the fiber direction $\boldsymbol{\mu}$ and (iii) κ can be interpreted as a measure of anisotropy of the diffusion. The latter can be related to the fractional anisotropy (FA) [4] as $\text{FA} = \kappa\left[(\kappa+1)^2 + 2\right]^{-1/2}$. We refer the reader to [2] for more details about the motivations of such a parametrization.

The probability density function (pdf) of the molecular displacement $\boldsymbol{x} - \boldsymbol{x}_0$ is then obtained by the convolution of the von Mises & Fisher pdf and the Gaussian pdf, and is parametrized by the four parameters $\{\theta, \phi, \kappa, R\}$.

Multi-compartment Model Due to its low number of parameters, the single-compartment model is particularly suited to be encompassed within a multi-compartment model, which can account for more than one fiber direction within each voxel. We thereby model the pdf of molecular displacements as a mixture of pdfs having the common parametric form proposed in the previous section.

We assume m compartments associated with m different fiber directions $\boldsymbol{\mu}_i$ $(i = 1, \ldots, m)$. In each compartment, the diffusion is modeled according to the previously described pdf with parameters $\{\boldsymbol{\mu}_i, \kappa_i, R_i\}$ and mixture weight FA_i/m. We also include an additional pdf in the mixture, with weight $1 - \sum_{i=1}^{m} \text{FA}_i/m$ to account for isotropic diffusion; this pdf follows the general form with $\kappa = 0$, so that the unique remaining parameter to estimate is R_0. Furthermore, we set $R_i^2 = (\kappa_i + 1)\lambda$, $\forall i \in [\![1, m]\!]$, where $\lambda > 0$ is the transverse diffusivity assumed identical in each compartment. For more details about the above described parametrization, we invite the reader to see [2]. Considering m putative fiber directions with this parametrization yields a m-compartment DDI model with $3m + 1$ parameters.

Estimation of the DDI Parameters The theoretical diffusion weighted intensities are the modulus of the Fourier transform of the pdf of molecular displacements which can be analytically derived under the assumption of the DDI model

[2]. The $3m+1$ unknown parameters of the m-compartment DDI model are then **estimated** using a least squares fitting on the raw diffusion weighted intensities, and this **optimization** is performed using the derivative-free NEWUOA optimization algorithm [5]. The different compartments are sorted in decreasing order according to their κ. The model selection is performed according to the procedure described in [2].

2.2 Tractography Algorithm

Our goal is to track the fibers linking multiple regions of interest (ROIs). To this end, we developed a deterministic streamline algorithm, which can be viewed as an extension of the original FACT method [6], adapted to the DDI model, using a *breadth-first*-type search.

Starting from one of the ROIs, we define one starting point at each voxel of the ROI. Given one point along its path, we build the *main* fiber iteratively as follows:

1. If the number of putative fiber directions $m = 0$, we stop the tracking.
2. If $m = 1$, we compute FA_1 and the angle α_1 between the input direction and $\boldsymbol{\mu_1}$. If $\alpha_1 < \alpha_t$ and $FA_1 > FA_t$, then we follow the single putative fiber direction $\boldsymbol{\mu_1}$ with a step size of l millimeters. Else, we stop the tracking.
3. If $m = 2$, we compute FA_1, FA_2, the angle α_1 (resp. α_2) between the input direction and $\boldsymbol{\mu_1}$ (resp. $\boldsymbol{\mu_2}$). If:
   - $\alpha_t < \alpha_1, \alpha_2$: we stop the tracking.
   - $\alpha_1 < \alpha_t < \alpha_2$: cf. the case $m = 1$.
   - $\alpha_2 < \alpha_t < \alpha_1$: if $FA_2 > FA_t$, then we follow the direction $\boldsymbol{\mu_2}$ with a step size of l millimeters, else we stop the tracking.
   - $\alpha_1, \alpha_2 < \alpha_t$: if $FA_2 < FA_t$, then cf. the case $m = 1$; else if $\kappa_2 > r \times \kappa_1$ then we sort the two fibers in ascending order according to the angles α_i. We follow the new direction $\boldsymbol{\mu_1}$ with a step size of l millimeters and we record the second putative fiber direction $\boldsymbol{\mu_2}$ (*branch*) for future use, as it can be indicative of crossing/kissing/merging/diverging fibers.

Once we have tracked this main fiber, we perform the same tracking from all the possible branching points that we have recorded along its path. Importantly, for these trackings, the stepping rule and stopping criteria are identical as those for the main fiber, but we do not record any possible mixed fiber configuration along these secondary paths, for which we only follow the main direction $\boldsymbol{\mu_1}$ at each step. We then lead the same tracking from the other ROIs. We only keep the tracts going through all the seeding ROIs for further analysis. In practice, we choose the parameters $l = 1$, $r = 0.8$, $\alpha_t = 60$ degrees (maximal angle between two successive directions along the fiber) and $FA_t = 0.5$ (minimal FA along the fiber). During the tracking, when a point is not on the grid of the DW-MR images, we compute the DDI model using a trilinear interpolation directly on the model parameters.

2.3   Tractography Pipeline Applied to the Challenge Datasets

We utilize the following processing pipeline to extract the CST for the challenge datasets. An expert neuroanatomist (Romuald Seizeur) delineated two ROIs on each side (left and right) of the original T1-weighted images. One is located in the posterior limb of the internal capsule and the other in the superior part of the mesencephalon. In addition, since crossing fiber tracts such as the association or commissural fiber tracts may be considered as bifurcations of the CST by the tractography algorithm, the same expert also delineated regions through which the tracts are not allowed. On the patients' datasets, the same ROIs were delineated with some modifications to account for the deformations caused by the tumor (e.g. in patient 1 the internal capsule on the left side is compressed by the infiltrating tumor).

All datasets were then processed in three steps:

1. Diffusion-weighted MRI denoising: DW-MRI is subject to random noise yielding measures that are different from their real values, and thus biasing the subsequently estimated diffusion models. We filtered the diffusion-weighted MR images with the Rician-adapted Non-Local Means filter [7], which has been shown to efficiently denoise such images while preserving fine anatomical structures. In particular, this filter has also been shown to preserve the angular resolution of q-ball ODF models estimated from HARDI data [8].
2. ROI alignment on B0 images: we registered the ROIs on the B0 images according to the following steps:
   - global affine registration of the T1-weighted images to the B0 images [9];
   - cropping of the affine-registered T1-weighted images using the mask of the B0 images;
   - constrained non-rigid registration [10] of the masked T1-weighted images to the B0 images;
   - application of the obtained transformations to the ROIs.
3. Extraction of the left and right CST using the aligned ROIs and the DDI estimated from the DWI.

3   Results

The MICCAI DTI tractography challenge consists of two groups of data: two healthy subjects acquired using a multiple b-values scheme and two patients acquired using a more standard acquisition protocol. For each of the two healthy subjects, DW-MRI data were acquired repeatedly (ten repetitions) so that the reproducibility of the tractography method may be evaluated. On the other hand, the tumors of the two patients were delineated so that we could produce combined views to help the surgeon, for example when planning a tumor removal surgery.

3.1 Tractography on Healthy Subjects

For each of the repetitions of each subject, the left and right CST were computed utilizing the aligned ROIs (see Section 2.3). We display the tractography of one volume of each of the two subjects in Fig. 1.
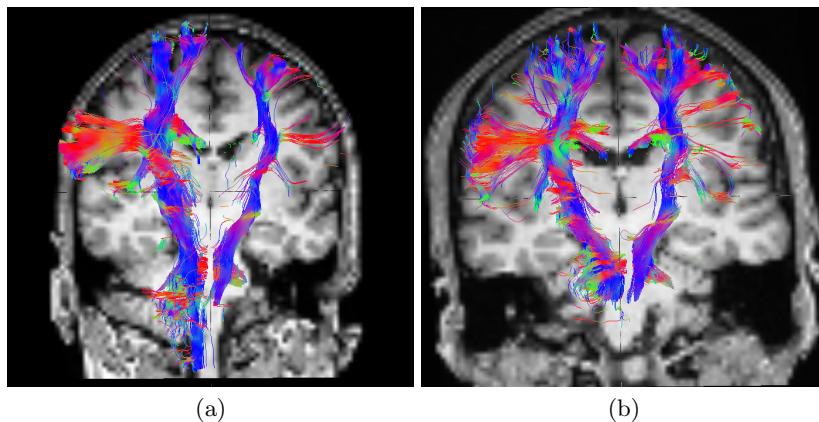

(a)   (b)

Fig. 1. Illustration of CST on Healthy Subjects. Representative examples of obtained fiber tracts for healthy subject 1 (a) and 2 (b) (T1 images are in radiological conventions, i.e. the left hemisphere is on the right side of the image). To see the full extent of fiber spreading, all 3D fiber tracts are displayed. This explains why they may not seem to match exactly the background T1 image.

This figure illustrates that we are able to cover the full extent of the CST for these healthy subjects, from the face area to the hand area to the medial part of the CST. This demonstrates that our diffusion model enables the tractography algorithm to follow bifurcations in the white matter fiber tracts. For each subject, estimating the DDI models from the DWI took approximately 40 minutes (single-threaded), while the tractography of the left and right CST took less than ten minutes.

3.2 Tractography on Patients

We also report results for the CST of each patient on the side of the tumor (all fiber bundles are provided in supplemental material). The images processed here had a larger resolution than the healthy subjects and the estimation of the DDI models from the DWI took approximately 3 hours (single-threaded). However, this step of the tractography pipeline may be computed offline leaving only the tractography to perform online (about five minutes for each CST) when performing the tractography for surgery planning.

We focus on the qualitative evaluation of the obtained tracks and their closeness to the tumor (it should be noted that the tumor regions were not used in
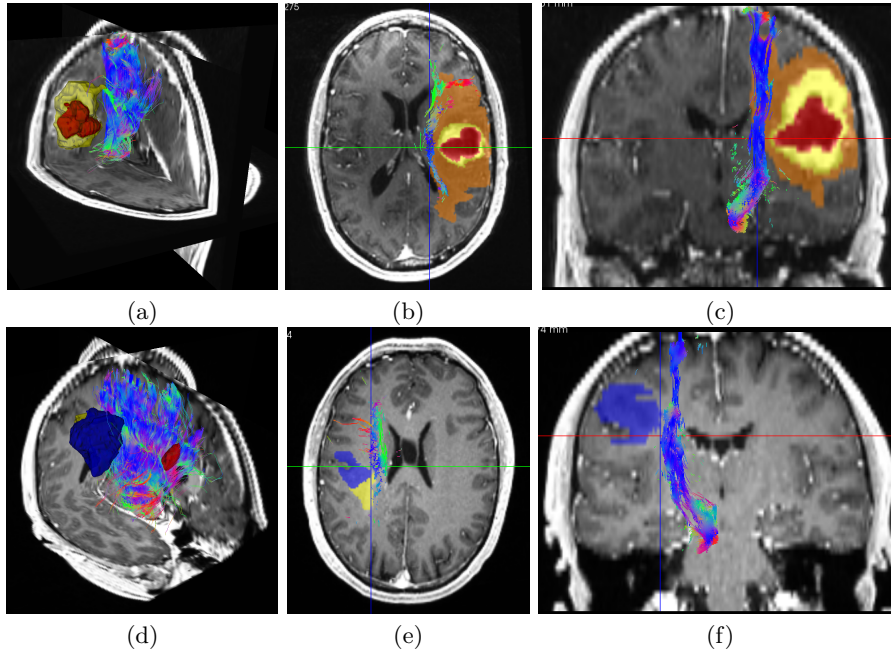
Fig. 2. Illustration of CST on Patients. Combined views of the obtained fiber tracts for patients 1 (a,b,c) and 2 (d,e,f), illustrating the proximity of the tumor to crucial motor pathways. Surfaces for the first patient correspond to the necrotic part of the tumor (red), the active part of the tumor (yellow) and the edema (orange). For the second patient, each ROI corresponds to a specific tumor. Images (a,d) show overall 3D views and (b,c,e,f) show the tracts and regions of interest going through a specific 2D slice to better illustrate their proximity.

any way to constrain the tractography algorithm), and on providing the neurosurgeon with helpful views for neurosurgery planning. To this end, we present in Fig. 2 views (made using the MedINRIA software [11]) combining the fiber tracts, the tumor ROIs provided by the organizers, all on top of the patient's T1 image. More illustrations are available in supplemental material.

We can observe on this figure that, although the tumor delineation was not used in the algorithm, no fibers are going through the tumor area on patient 1. Instead, the CST is going through the most central part of the edema (see images (b,c) on Fig. 2). This indicates that the fibers were pushed by the tumor mass effect, which is a valuable indication when planning the surgery. Overall, this figure demonstrates the close proximity of the tumors and of the CST for both patients. This is an important insight as the neurosurgeon will be able to plan the tumor removal in the optimal way, so as to minimize the possible handicap for the patient after surgery.

References

1. Behrens, T.E.J., Berg, H.J., Jbabdi, S., Rushworth, M.F.S., Woolrich, M.W.: Probabilistic diffusion tractography with multiple fibre orientations: What can we gain? Neuroimage **34**(1) (January 2007) 144–155
2. Stamm, A., Pérez, P., Barillot, C.: Diffusion directions imaging. Research Report RR-7683, INRIA (2011)
3. Friman, O., Westin, C.F.: Uncertainty in white matter fiber tractography. In: MICCAI. (2005) 107–14
4. Basser, P.J., Pierpaoli, C.: Microstructural and physiological features of tissues elucidated by quantitative-diffusion-tensor MRI. Journal of magnetic resonance. Series B **111**(3) (June 1996) 209–19
5. Powell, M.: The NEWUOA software for unconstrained optimization without derivatives. In Pardalos, P., Pillo, G., Roma, M., eds.: Large-Scale Nonlinear Optimization. Volume 83 of Nonconvex Optimization and Its Applications. Springer US (2006) 255–297
6. Mori, S., Crain, B.J., Chacko, V.P., van Zijl, P.C.: Three-dimensional tracking of axonal projections in the brain by magnetic resonance imaging. Ann Neurol **45**(2) (February 1999) 265–269
7. Wiest-Daesslé, N., Prima, S., Coupé, P., Morrissey, S.P., Barillot, C.: Rician noise removal by non-local means filtering for low signal-to-noise ratio MRI: applications to DT-MRI. In: MICCAI, New York, United States (2008) 171–9
8. Descoteaux, M., Wiest-Daesslé, N., Prima, S., Barillot, C., Deriche, R.: Impact of Rician Adapted Non-Local Means Filtering on HARDI. In: MICCAI. (2008) 122–30
9. Ourselin, S., Roche, A., Prima, S., Ayache, N.: Block matching: A general framework to improve robustness of rigid registration of medical images. In: MICCAI. (2000) 557–66
10. Garcia, V., Commowick, O., Malandain, G.: A Robust and Efficient Block Matching Framework for Non Linear Registration of Thoracic CT Images. In: MICCAI'2010 Grand Challenges in Medical Image Analysis Workshop. (2010)
11. Toussaint, N., Souplet, J., Fillard, P.: MedINRIA: Medical Image Navigation and Research Tool by INRIA. In: MICCAI'2007 Workshop on Interaction in Medical Image Analysis and Visualization. (2007)

Automated atlas-based seeding in cortico-spinal tractography

Maged Goubran[1,2], Ali R. Khan[2], Sandrine de Ribaupierre[3], and Terry M. Peters[1,2]

[1] Imaging Research Laboratories, Robarts Research Institute,The University of Western Ontario, London, Ontario, Canada
[2] Department of Biomedical Engineering,The University of Western Ontario, London, Ontario, Canada
[3] Department of Neurosurgery,The University of Western Ontario, London, Ontario, Canada

Abstract. Providing neurosurgeons with visualization-based guidance has a great potential to improve surgical outcomes. We present here a pipeline for extraction of the cortico-spinal tract using automated atlas-based seeding with a single-subject atlas. Our protocol uses the Colin27 single-subject atlas along with fast non-rigid brain registration to automatically generate label-based seeds for tractography. The pre and post-central gyri labels from the atlas were used as seeds. A manually delienated cerebral peduncle label as well as other Colin27 labels were used, in ROI based selection and removal of fibres, to eliminate false-positive tracks. A set of tractography parameters were chosen in order to reliably generate the nerve fibres. In only less than 10% of the cases, the chosen parameters were not sufficient for prevention of false-positive tracts and were optimized. Our method is an automated labelmap seeding with multi ROI filters that averts inter and intra subject variability, thus offering a high reproducibility in generating accurate cortico-spinal tracts.

1 Introduction

Tractography using Diffusion Tensor Imaging (DTI) has the potential to significantly impact neurosurgical procedures. Operations involving the resection of tissue or tumour can damage eloquent areas within the brain. Thus, providing the neurosurgeon with visualization-based guidance and possibly tracking can improve surgical outcomes.

Many tractography approaches have been based on brute force (streamlines from every voxel) with user-defined seeds or regions of interest (ROIs) and pruning of fiber bundles [1–3], which can suffer from rater reliability issues. Automated labelling techniques based on brain registration have the advantage of generated a full set of brain labels for automated seed selection by warping labels from an atlas. Our submission uses a labelled atlas along with fast non-rigid brain registration to automatically generate label-based seeds for tractography in order to segment the cortico-spinal tract.

2 Methods

2.1 Imaging

MRI datasets were provided by the workshop organizers and were obtained from the Department of Neurosurgery at Brigham and Women's Hospital, Boston, MA, with repeat control scans from the Scientific Computing and Imaging Institute, Salt Lake City, Utah. Each set contained diffusion weighted images (DWI) (25 directions plus the baseline), Diffusion Tensor Images (DTI), and registered T1/T2-weighted anatomical images. Our processing pipeline began with the DTI images and made use of the T1 anatomical images for atlas registration.

2.2 Atlas-based labelling

The Colin27 single-subject atlas [4] was used for atlas-based labelling of seed regions in each subject. The freely available Freesurfer Image Analysis Suite http://surfer.nmr.mgh.harvard.edu/fswiki/ was used for automated labelling of the atlas, generating subcortical segmentations [5] and voxelized cortical parcellations [6]. In addition, the cerebral peduncles were manually segmented in the atlas MRI.

2.3 Atlas registration

The Colin27 atlas was registered to each individual subject scan using a two stage rigid/affine to non-rigid registration procedure as implemented in the freely available Nifty Reg http://sourceforge.net/projects/niftyreg toolkit.

The rigid/affine registration algorithm uses a block-matching approach, that relies on trimmed least squares for robustness to outliers [7]. In this scheme the block matching first provides a set of corresponding points, which are then used to find the best global rigid/affine transformation between the images using a normalized cross-correlation image similarity metric. These two steps are repeated until convergence by a multi-resolution scheme.

The non-rigid algorithm [8] is a GPU-enabled implementation based on the free-form deformation B-spline algorithm by Rueckert et al. [9]. A normalized mutual information image similarity metric is used along with a bending energy for regularization. The lattice of control points is successively increased for a multi-resolution approach.

Following generation of the non-rigid deformation field, the automated and manual labels in the Colin27 atlas were propagated to the subject space using nearest-neighbour interpolation. The labels for precentral and postcentral gyri were dilated once to ensure overlap with the cortical white-matter tissue. Figure 1 shows the Colin27 atlas and the labels in the healthy subject 1 space.

(a) Colin27 MRI   (b) Colin27 Freesurfer   (c) hs1 Labelled
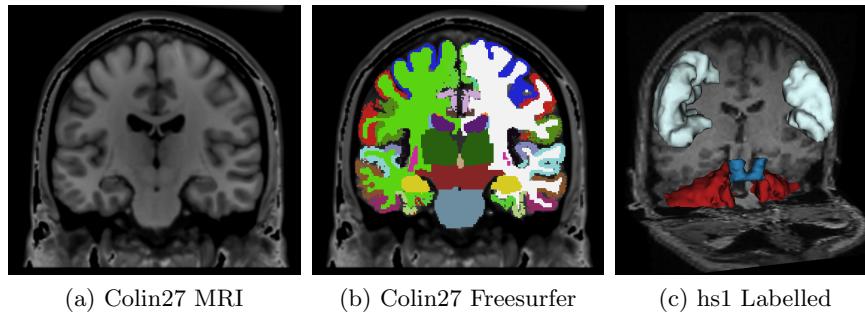
Fig. 1: Visualizations of (a) Colin27 atlas MRI, (b) Freesurfer labels, and (c) a healthy subject with atlas-based labels (pre and post-central gyri, cerebral peduncles, and cerebellum), used for seeding and selecting tracts.

2.4 Tractography

Tractography was performed in the open source software 3D Slicer, version 3.6.3 (http://www.slicer.org[10]) using the Labelmap Seeding and ROI Select modules to generate the cortico-spinal tract fibre bundles. The procedure for extracting the corticospinal tract in a given hemisphere consisted of 1) labelmap seeding using the combined and dilated precentral and postcentral labels (parameters in Table 1), 2) ROI-based selection of the generated tracts that run through the cerebral peduncle label, and 3) ROI-based removal of the tracts that run through the cerebellum and white matter from the opposite hemisphere. In less than 10% of the cases the chosen parameters were not sufficient for prevention of false-positive tracts and thus the minimum length or curvature were increased in these cases. The image-based envelope of the tracts were generated using the ModelIntoLabelVolume module.

Parameter	Value
Seed spacing	0.8 mm
Linear Measure Start Threshold	0.3
Minimum Tract Length	100 mm
Maximum Tract Length	200 mm
FA Stop Threshold	0.1
Curvature Stop Threshold	0.85
Integration Step Length	0.5 mm

Table 1: Parameters used for label-based tract seeding in Slicer3.

Patient tumour and tractography visualizations, shown in Figure 2, were generated using models of the tumours (Patient1 models were provided by the

workshop organizers), a skull-stripped volume as well as a cortical surface visualization of the brain. Skull-stripped was performed using the Brain Extraction Tool (BET) in FSL (http://www.fmrib.ox.ac.uk/fsl/ [11])and the cortical surface was acquired from the Freesurfer Image Analysis Suite. The total processing time for each neurosurgical case was under 10 min, which includes the time taken for atlas based segmentation of ROIs, seeding the tracts, ROI based selection and removal of fibers, as well as time for generating the tumour models [it should noted that this time does not include manually delineating the tumours for label creation].
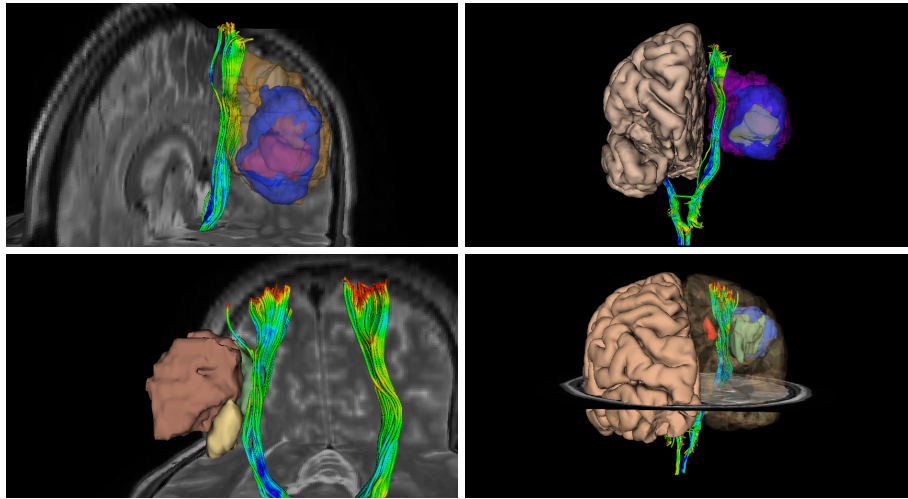
Fig. 2: Visualization of patient1 tractography with tumours and edema present for neurosurgical guidance (Top: Patient1, Bottom: Patient2)

3   Appendix: Evaluation criteria

Quantitative reference-based similarity measures for tractography are ideal for evaluating methodologies, however, this is inherently dependent on the existence of an accurate and reliable reference. Gold standard tractography is elusive because of the noise present in the DWI images, the and the deterministic nature of streamline-based tractography methods that may falsely capture the noise. Furthermore, applying tractography without functional evidence may produce tracts which look anatomically meaningful but are not functionally accurate.

To deal with the problem of noisy data, one can apply a co-registration and averaging approach to fuse multiple DWI acquisitions into a single high SNR DWI dataset. The healthy subject datasets used in this workshop could be used

to produce such as dataset, which would correspondingly produce a more robust estimate of the diffusion tensors.

Secondly, to ensure spatially accurate seeding, blood-oxygen level dependent (BOLD) fMRI could be used to map, for example, the motor cortex by using a button-press paradigm. The combined reduction of noise and improvement in localization of seed points should result in an in-vivo reference tractography that approaches gold-standard.

References

1. Mori, S., Crain, B.J., Chacko, V.P., van Zijl, P.C.: Three-dimensional tracking of axonal projections in the brain by magnetic resonance imaging. Ann Neurol **45**(2) (1999) 265–9
2. Basser, P.J., Pajevic, S., Pierpaoli, C., Duda, J., Aldroubi, A.: In vivo fiber tractography using DT-MRI data. Magn Reson Med **44**(4) (2000) 625–32
3. Jones, D.K., Simmons, A., Williams, S.C., Horsfield, M.A.: Non-invasive assessment of axonal fiber connectivity in the human brain via diffusion tensor MRI. Magn Reson Med **42**(1) (1999) 37–41
4. Holmes, C.J., Hoge, R., Collins, L., Woods, R., Toga, A.W., Evans, A.C.: Enhancement of MR images using registration for signal averaging. J Comput Assist Tomogr **22**(2) (1998) 324–33
5. Fischl, B., Salat, D., Busa, E., Albert, M., Dieterich, M., Haselgrove, C., van der Kouwe, A., Killiany, R., Kennedy, D., Klaveness, S.: Whole brain segmentation: automated labeling of neuroanatomical structures in the human brain. Neuron **33**(3) (2002) 341–355
6. Fischl, B., van der Kouwe, A., Destrieux, C., Halgren, E., Ségonne, F., Salat, D.H., Busa, E., Seidman, L.J., Goldstein, J., Kennedy, D., Caviness, V., Makris, N., Rosen, B., Dale, A.M.: Automatically parcellating the human cerebral cortex. Cereb Cortex **14**(1) (2004) 11–22
7. Ourselin, S., Roche, A., Prima, S., Ayache, N.: Block matching: A general framework to improve robustness of rigid registration of medical images. MICCAI 2000 **LNCS 1935** (2000) 557
8. Modat, M., Ridgway, G.R., Taylor, Z.A., Lehmann, M., Barnes, J., Hawkes, D.J., Fox, N.C., Ourselin, S.: Fast free-form deformation using graphics processing units. Computer methods and programs in biomedicine **98**(3) (2010) 278–84
9. Rueckert, D., Sonoda, L.I., Hayes, C., Hill, D.L., Leach, M.O., Hawkes, D.J.: Non-rigid registration using free-form deformations: application to breast MR images. IEEE Transactions on Medical Imaging **18**(8) (1999) 712–21
10. Gering, D.T., Nabavi, A., Kikinis, R., Hata, N., O'Donnell, L.J., Grimson, W.E., Jolesz, F.A., Black, P.M., Wells, W.M.: An integrated visualization system for surgical planning and guidance using image fusion and an open MR. J Magn Reson Imaging **13**(6) (2001) 967–75
11. Smith, S.M.: Fast robust automated brain extraction. Human Brain Mapping **17**(3) (2002) 143–155

MITK Global Tractography - Application to the Corticospinal Tract

Peter F. Neher[1], Bram Stieltjes[2], Marco Reisert[3], Ignaz Reicht[1], Hans-Peter Meinzer[1], and Klaus H. Fritzsche[1,2,★]

[1] German Cancer Research Centre, Division of Medical and Biological Informatics,
Im Neuenheimer Feld 280, 69120 Heidelberg, Germany
[2] German Cancer Research Center, Division of Radiology,
Im Neuenheimer Feld 280, 69120 Heidelberg, Germany
[3] University Hospital Freiburg, Dept. of Radiology, Medical Physics,
Breisacher Straße 60a, 79106 Freiburg, Germany

Abstract. In the DTI Tractography Challenge MICCAI 2011 different tractography algorithms compete in tracking the corticospinal tract. In this paper we present an implementation of the global tractography algorithm proposed by Reisert *et.al.* [1] using the open source Medical Imaging Interaction Toolkit (MITK) developed and maintained by the Division of Medical and Biological Informatics at the German Cancer Research Center (DKFZ). The MITK diffusion imaging application combines all the steps necessary for a successful tractography: preprocessing, reconstruction of the images, the actual tracking, live monitoring of intermediate results, postprocessing and visualization of the final tracking results.

Keywords: Global Tracking, Neuronal Tractography, Diffusion-weighted Imaging, Q-Ball Imaging, Diffusion Tensor Imaging

1 Introduction

Up to now, diffusion weighted imaging (DWI) is the only technique to noninvasively gain insight into the architecture of the human white matter pathways. Tractography algorithms try to explicitly estimate the underlying fiber pathways from the given voxelwise information.
There exists a wide variety of different tractography algorithms that can be roughly divided into the two subgroups of local and global methods. Local methods try to reconstruct one fiber at a time by following the voxelwise information and successively adding segments to the fiber. Fibers can either be generated following a model-based or a model-free approach. While local methods are known to be performant, they often struggle with image artifacts or complex fiber configurations like crossings or kissings. Global methods try to reconstruct all fibers simultaneously, searching for a global optimum. While computationally much

---

★ Corresponding author. E-mail address: k.fritzsche@dkfz-heidelberg.de.

more challenging, global methods promise more robust results.

This work presents the integration of the successful [2] and also computationally efficient global approach proposed by Reisert *et.al.* [1] within the Medical Imaging Interaction Toolkit (MITK) developed at the German Cancer Research Center (DKFZ) and its application to reconstruct the corticospinal tract. MITK is a free open-source software system for development of interactive medical image processing software [3]. The diffusion imaging application is available on www.mitk.org and we are in the process of publishing it open source. This paper describes the processing pipeline that was applied to the datasets provided by the organizers of the DTI Tractography Challenge MICCAI 2011 to obtain tractography results of the corticospinal tract (CST).

2   Materials and Methods

Three steps were performed in order to obtain the desired reconstruction of the CST. The first step includes preprocessing and generation of additional information like mask images. The second step consists of the actual tractography and the third step describes the extraction of the corticospinal tract from the whole brain tracking result. The process is illustrated in Fig. 1.
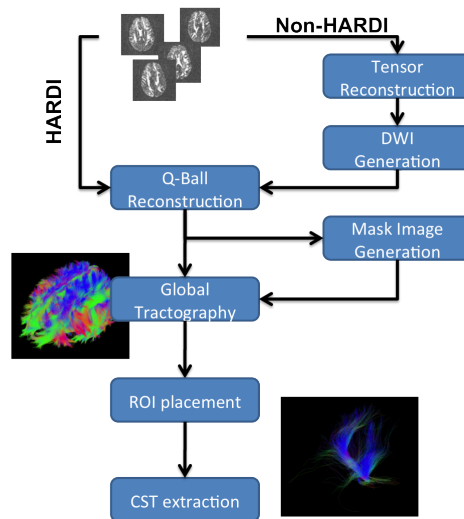

Fig. 1. Flowchart of the processing steps from DWI images to the extracted CST.

2.1   DWI Processing Pipeline

Depending on the type of acquisition, different reconstruction methods for the DWI can be chosen. Our tractography algorithm expects ODFs as input data.

If the DWI is already captured using a high angular resolution diffusion imaging (HARDI) sequence, the Q-Ball reconstruction can be performed directly. Otherwise a standard tensor reconstruction is applied and a new DWI image with high angular resolution is estimated from the tensor image. The resulting DWI image can then be processed via Q-Ball reconstruction.

In this work, the supplied DTI datasets were used directly instead of a reconstruction of the tensor data from the provided DWI datasets. There are several different Q-Ball reconstruction methods available in MITK like a numerical reconstruction (Tuch *et.al.* [4]) or a spherical harmonics reconstruction with solid angle consideration (Aganj *et.al.* [5]). In this work we used a basic spherical harmonics reconstruction as proposed by Descoteaux *et.al.* [6]. The applied tracking approach does not need a mask image to yield accurate tracking results, but by limiting the search space with a binary brain mask, the process can be accelerated considerably. The mask image was generated by a simple thresholding of the GFA image generated from the reconstructed Q-Ball image. The thus produced Q-Ball and mask images are used as input for the tracking algorithm.

2.2   Global Tractography

The basic idea of the global tractography algorithm [1] is to fit a model M, consisting of directed points (particles) and connections between the particles, to the image data D by minimizing two energy terms.

The first energy, the so called external energy E_{ext}, measures the distance from the artificial signal ρ_M computed from the current model configuration to the original image data, i.e. the external energy ensures that M is able to explain the signal in the best possible way. The external energy is computed as

$$E_{ext}(M, D) = \lambda_{ext}||\rho_M - D||^2_{L_2(\mathbb{R}^3 \times S_2)}, \tag{1}$$

where λ_{ext} is a weighting factor controlling the balance between external and internal energy.

The second energy, the internal energy E_{int}, applies certain constraints to the model itself. It is designed to enforce long and straight fibers. By minimizing E_{int} the model is shaped in a way that is consistent with structural knowledge about neuronal fibers. Each particle can connect to another particle with one of its endpoints. A chain of connected particles represents a fiber. The connection potential between two particles is small if the endpoints of two connected particles lie close together and point in the same direction.

To optimize the model, the whole problem is formulated as a maximization of the a-posteriori probability of the model M given the image data D:

$$P(M|D) = exp(-E_{int}(M)/T - E_{ext}(M, D)/T), \tag{2}$$

$P(M|D)$ is maximized via the introduction of random change proposals with a certain probability p_{prop} into the model M. The resulting model configuration M' is afterwards accepted or rejected according to a certain ratio calculated from $P(M'|D)$ and $P(M|D)$. By successively reducing the temperature T it becomes

more and more likely to converge to a steady and optimal configuration of the model. For more details regarding the algorithm, please refer to [1].

To increase the number of detected fibers and to account for the statistical nature of the process, each image was tracked four times with 10^8 iterations for each image and the results were combined afterwards.

2.3   Extraction of the Corticospinal Tract

The tractography approach described in the previous subsection yields a whole brain tracking result. To extract the CST from the whole brain result seven ROIs were placed manually. The first ROI ($R1$) is placed in a tranversal slice on the brain stem at about the height of the Pons, while catching both strands of the corticospinal tract and avoiding the Superior Cerebellar Peduncle and the Medial Lemniskus. The second and third ROI ($R2$, $R3$) are placed on the posterior limb in the internal capsule of the respective hemisphere to catch the fibers spreading out to form the Corona Radiata. The fourth ROI ($R4$) is placed sagittally between the two hemisphere to catch and erase fibers crossing the Corpus Callosum. The three ROIs $R5 - R7$ are placed left, right and behind the lower part of the CST to erase the remaining fibers of the Superior Cerebellar Peduncle and the Medial Lemniskus. The ROIs were placed similarly for all 22 images. A schematic ROI placement of $R1 - R6$ is depicted in Fig. 2 ($R7$ was omitted in this figure due to clarity issues). The ROIs are combined via logical operations to extract or avoid fibers respectively in the following manner:

$$R = R1 \wedge (R2 \vee R3) \wedge \neg(R4 \vee R5 \vee R6 \vee R7) \qquad (3)$$

All fibers that do not pass through the composite ROI R are removed.

3   Results

The method described in chapter 2 was applied to all provided 22 diffusion tensor images obtained from four different probands. Ten images each were obtained from two healthy subjects and one image from two surgical cases respectively.

In all images the corticospinal tract was detected successfully. Figure 3 shows the sagittal and coronal tracking results of all 22 images. Fig. 4 shows the whole brain tracking result of the patient 1 dataset as well as the according extracted CST and ROIs used for the extraction in four different views.

4   Discussion and Conclusion

In this paper we presented tracking results of the CST using MITK global tractography. The CST was successfully tracked in the diffusion weighted images supplied by the Organizers of the DTI Tractography Challenge MICCAI 2011. Surprisingly some branches of the corona radiata of the CST were detected more satisfying in the healthy subject datasets which are of much lower resolution
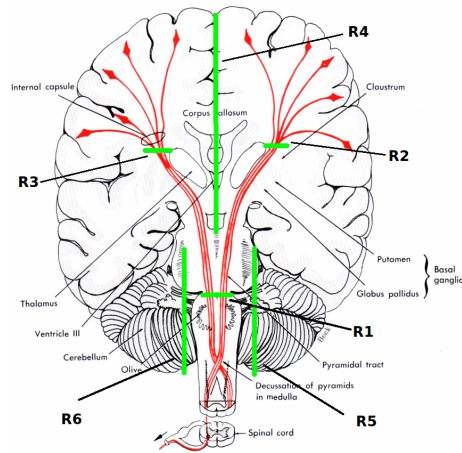
Fig. 2. Schematic placement of the ROIs (green) used to extract the corticospinal tract from the whole brain tracking (R7 omitted). Image adapted from [7]

and quality than the two neurosurgical datasets. A qualitative evaluation of the according region lead to the conclusion that the image data of the two neurosurgical subjects in fact does not supply the information needed to reconstruct the according fiber tracts. The issue is illustrated in Fig. 5.

References

1. Reisert, M., Mader, I., Anastasopoulos, C., Weigel, M., Schnell, S., Kiselev, V.: Global fiber reconstruction becomes practical. Neuroimage **54** (2011) 955–962
2. Fillard, P., Descoteaux, M., Goh, A., Gouttard, S., Jeurissen, B., Malcolm, J., Ramirez-Manzanares, A., Reisert, M., Sakaie, K., Tensaouti, F., Yo, T., Mangin, J.F., Poupon, C.: Quantitative evaluation of 10 tractography algorithms on a realistic diffusion MR phantom. Neuroimage **56**(1) (2011) 220–234
3. MITK.org: The Medical Imaging Interaction Toolkit MITK. [Online]. Available: http://www.mitk.org. [Accessed: April 12, 2011] (2005)
4. Tuch, D.S.: Q-Ball Imaging. Magnetic Resonance in Medicine **52** (2004) 1358–1372
5. Aganj, I., Lenglet, C., Sapiro, G.: Odf reconstruction in q-ball imaging with solid angle consideration. In: Sixth IEEE International Symposium on Biomedical Imaging. (2009)
6. Descoteaux, M., Angelino, E., Fitzgibbons, S., Deriche, R.: Regularized, Fast, and Robust Analytical Q-Ball Imaging. Magnetic Resonance in Medicine **58** (2007) 497510
7. arthursclipart.org: Corticospinal Tract. ([Online]. Available: http://www.arthursclipart.org [Accessed: June 7, 2011])
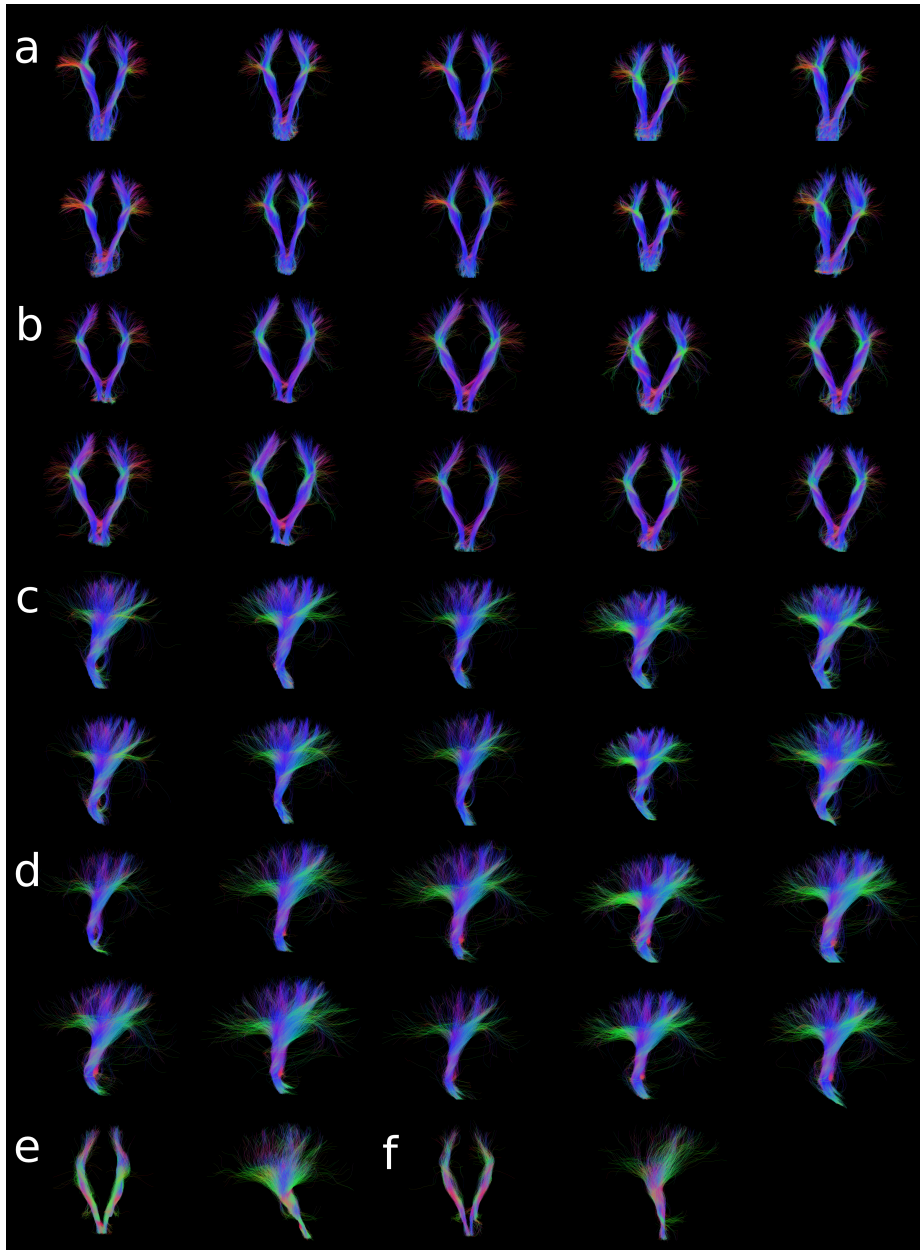
Fig. 3. (a) CST tracking of healthy subject 1 (coronal view) (b) CST tracking of healthy subject 2 (coronal view) (c) CST tracking of healthy subject 1 (sagittal view) (d) CST tracking of healthy subject 2 (sagittal view) (e) CST tracking of patient 1 (coronal and sagittal view) (f) CST tracking of patient 2 (coronal and sagittal view).
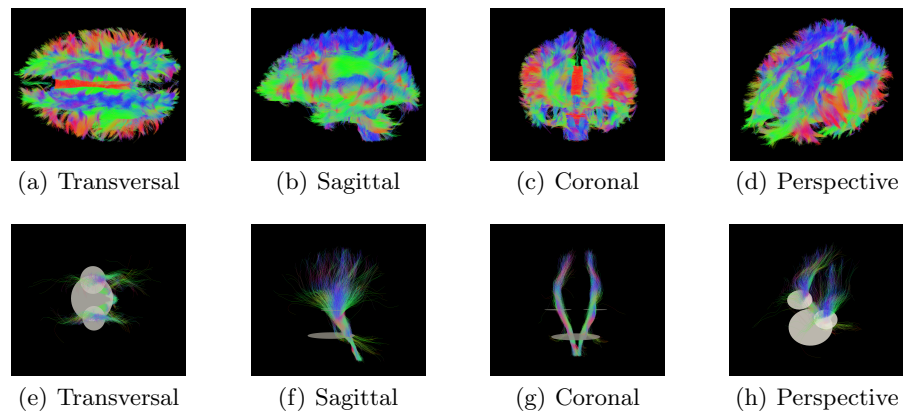
(a) Transversal   (b) Sagittal   (c) Coronal   (d) Perspective

(e) Transversal   (f) Sagittal   (g) Coronal   (h) Perspective

Fig. 4. a-d: Whole brain tractography result of the patient 1 dataset. e-h: CST tracts including ROIs used for the extraction (negative ROIs omitted).

(a) HS1 DTI and ROI   (b) HS1 Tensor Visualization   (c) HS1 3D Tractography

(d) PAT1 DTI and ROI   (e) PAT1 Tensor Visualization   (f) PAT1 3D Tractography
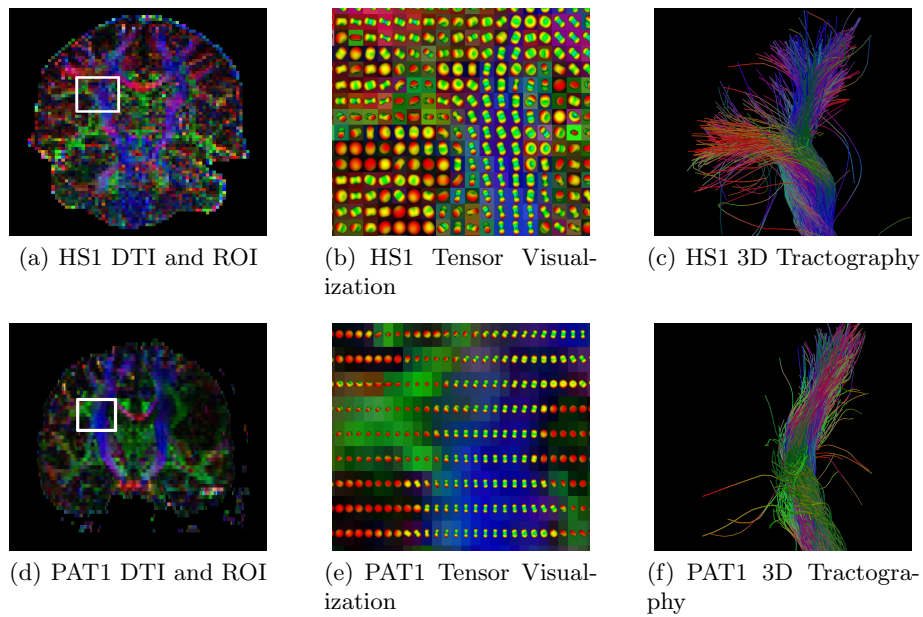
Fig. 5. Comparison between healthy subject 1 (upper row) and patient 1 (lower row) in the branching regions of the corona radiata. The left column (image (a) and (d)) show the coronal view of both images with a ROI marked as white rectangle. Image (b) and (e) depict the tensor visualization of the according ROI and the rightmost column (image (c) and (f)) shows the respective 3D visualization of the tracking result. The neurosurgical dataset does not seem to supply the information needed for a successful tracking of the branching.

Using Filtered Multitensor Tractography

Yundi Shi, Eric Malbie, Martin Styner

Department of Psychiatry, UNC - Chapel Hill

Abstract. This paper describes the pipeline that was applied to the data in the tractography grand challenge. It included 1) preprocessing of the data 2) seeding of the regions 3) applying the filtered two-tensor tractography method and 4) cleaning up of the fiber tracts manually in Slicer3 [1]. Each step was demonstrated with screen shots and a full list of parameters applied.

1 Introduction

This paper describes the pipeline used in the submission for MICCAI 2011 tractography grand challenge. Four major steps were performed in this pipeline including 1) Pre-processing of the data 2) Manual selection of the seeding region for tracking 3) Tracking with filtered multitensor tractography method 4) Manual cleaning of the tracts in Slicer3. The tracking method applied was developed based on previous developed filtered multitensor algorithm [1]. Two-tensor tractography method was chosen fo tracing the cortical-spinal tract as this tract connects the spianl cord and different cortical regions and has a lot of fanning and diverging fibers in nature which is always a challge for single-tensor based tractography methods. This method, however is sensitive to noise as is seen in the results.

2 Pipieline Description

2.1 Pre-processing

Two sets of patient data and two sets of healthy control data were provided for this tractography grand challenge. The two dataset for patient1 and patient2 were not pre-processed. The original dwi data was taken as the input to perform the tractography. 10 dwi dataset for either healthy control was included. In order to eliminate any bias in manual seeding region selection, each of the 10 dataset was co-registered. First, one set (template) was chosen in each of the 10 healthy control dataset randomly. Then, fractional anisotropy (FA) maps of the other nine dataset was registered to that of this chosen dataset using rigid body registration. Register-Images (http://www.slicer.org/slicerWiki/index.php/Modules:RegisterImages-Documentation-3.6) was used using normalized correlation between images and center of mass option was chosen as the initialization step for registration.

---

[1] www.slicer.org

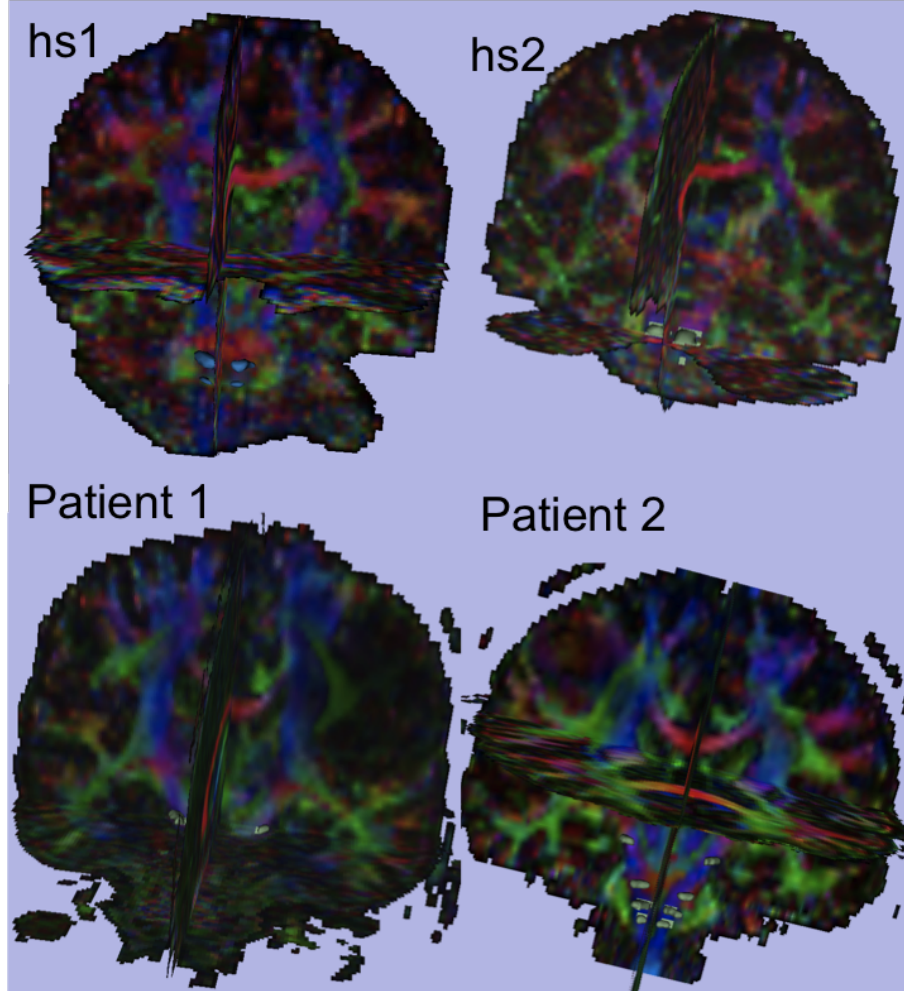## 2.2 Manual selection of the seed regions

Fig. 1. Manually selected seed regions in the patient data and one of the 10 healthy control dataset shown on color FA maps.

Bi-laterally regions were selected at the cerebral peduncle, and the pons and medulla regions as they are easy to identify in color FA maps. These regions were selected on 3 or 4 axial slices with the size of 10 voxels in general as shown in . Seed regions were manually selected in Slicer3 with the "Editor" modual. These regions were selected for both patient dataset and two of the template healthy control dataset. The seed region map for the healthy control dataset were then

propogated to each of the 10 healthy control dataset with inverse transformation as generated earlier.

2.3   Tracking with filtered multitensor tractography

Filtered multitensor tractography method was applied on all the dwi dataset in their original space. White matter masks were generated with simple thresholding of the FA maps. Step length of 0.5mm was used with 20 seeds per voxel in the selected seed regions. No branching was allowed.

2.4   Manual cleaning of the tracts withe Slicer3

ROISelect modual in Slicer3 (http://www.slicer.org/slicerWiki/index.php/Modules:ROISelect-Documentation-3.6) was used to manually clean the fiber tracts as the last step as shown in figure 2 .

References

1. Malcolm, J.G., Michailovich, O., Bouix, S., Westin, C.F., Shenton, M.E., Rathi, Y.: A filtered approach to neural tractography using the watson directional function. Medical Image Analysis **14**(1) (2010) 58 – 69
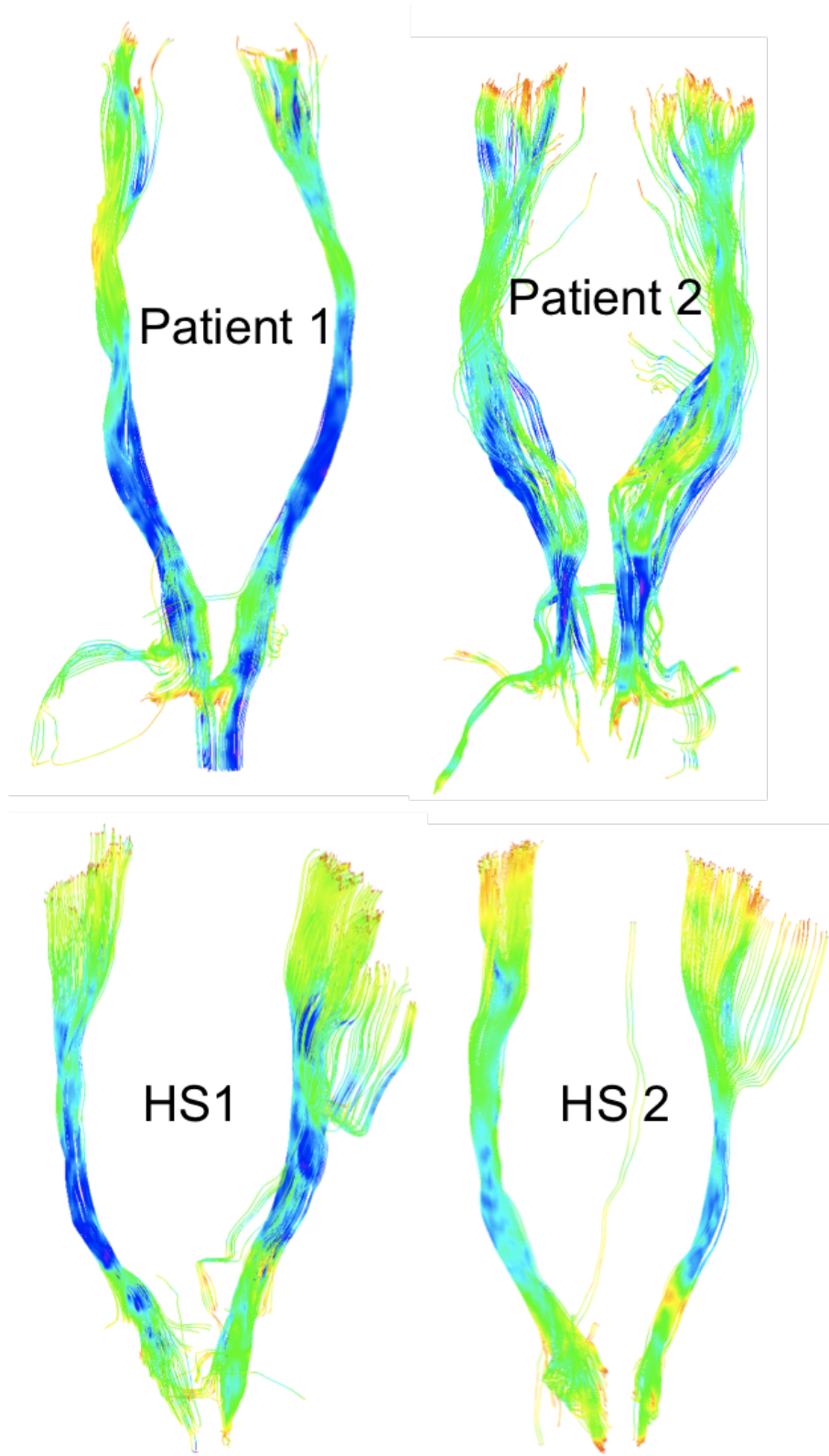
Fig. 2. Tracking results after manual cleaning. One of each10 healthy control (HS) dataset was chosen to represent the tracts.

DTI Tractography Challenge – MICCAI 2011: Global fiber-tracking based on Finsler distance

Antonio Tristán-Vega, Demian Wassermann, and Carl-Fredrik Westin

Laboratory of Mathematics in Imaging (Brigham and Women's Hospital, Boston)
{atriveg@bwh.harvard.edu,demian@bwh.harvard.edu,westin@bwh.harvard.edu}

1 Description of the algorithm [1]

This is a *global* fiber-tracking algorithm: to compute each point in the tract, not only the local diffusion information is considered, but instead we take into account all the voxels in the volume (or the ROI considered). Concretely:

- Let us define a seeding point (region) $\mathbf{x}_i$ and a target point (region) $\mathbf{x}_f$.
- Let us consider the set of all possible trajectories (fiber tracts estimated) Γ starting at $\mathbf{x}_i$ and ending at $\mathbf{x}_f$.
- The **local directional cost** $\phi(\mathbf{x}, \mathbf{d})$ is defined for all voxels $\mathbf{x}$ within the ROI, and for all possible unit directions $\mathbf{d}$ in the 3-D space.
- The Finsler distance between $\mathbf{x}_i$ and $\mathbf{x}_f$ is defined as (see Fig. 1):

$$D(\mathbf{x}_i, \mathbf{x}_f) = \min_{\Gamma} \int_{t_i}^{t_f} \phi\left(\Gamma(t), \frac{\Gamma'(t)}{\|\Gamma'(t)\|}\right) dt : \ \mathbf{x}_i = \Gamma(t_i); \mathbf{x}_f = \Gamma(t_f). \quad (1)$$

In other words: we sum $\phi(\mathbf{x}, \mathbf{d})$ at each point $\mathbf{x} \in \Gamma$ corresponding to the direction $\mathbf{d}$ tangent to Γ at $\mathbf{x}$. We need that the local cost depends on some property related to the diffusion: for a voxel $\mathbf{x}$, if the diffusivity along direction $\mathbf{d}$ is large, then $\phi(\mathbf{x}, \mathbf{d})$ should be small, i.e. the local directional cost is the inverse of the local directional diffusivity. Instead of using a diffusion tensor, we use a more general model based on Orientation Distribution Functions (ODF), which can represent complex scenarios like fiber-crossings. These functions are not represented as an ellipsoid but as a more general parametric function expressed in the basis of Spherical Harmonics (SH), see Fig. 1. Finally, to solve eq. (1) for Γ, the Fast Sweeping algorithm is used. It provides, for each voxel $\mathbf{x}$ within the ROI:

- The Finsler distance $D(\mathbf{x}_i, \mathbf{x})$, or **costs map**.
- The **arrival directions map**, i.e. the direction $\mathbf{d}$ tangent to Γ at $\mathbf{x}$.

For a given target point $\mathbf{x}_f$, we only have to back-trace (integrate) the arrival directions map from $\mathbf{x}_f$ to $\mathbf{x}_i$ to compute the fiber bundle joining $\mathbf{x}_f$ and $\mathbf{x}_i$[1].

---

[1] The code for the Fast Sweeping and the back-tracing is open-source and may be downloaded from http://www.nitrc.org/scm/?group_id=464.
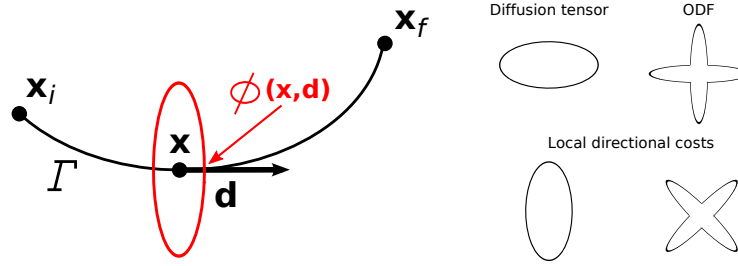
Fig. 1. Illustration of the Finsler method. **Left:** The optimal curve Γ is that minimizing the sum of $\phi(\mathbf{x}, \mathbf{d})$; these local directional costs are defined at each $\mathbf{x}$ and for each direction $\mathbf{d}$ (in the figure, the cost is the distance of the ellipsoid to its center). **Right:** Comparison of DTI and ODF models for diffusion; the local costs are the inverse of the diffusion functions. For a fiber-crossing, the cost for non-fiber directions is large.

2   Parameters of interest

The two main parameters to fix are:

- The sampling density of $\mathbf{d}$. The higher this density, the smoother the fibers and the more iterations the algorithm needs to converge. We use 60 orientations uniformly distributed in the sphere.
- The maximum degree of the SH (i.e. the precision) used to describe the ODF. The number of gradients of the data sets imposes a limit of $L = 4$, which is equivalent to using fourth order tensors.

3   Pros and cons

The algorithm has the following advantages:

- Compared to other *global* algorithms like stochastic tractography, this method is deterministic. For the same input volume and same parameters, it will always provide the same solution, favoring the reproducibility of the results.
- Stochastic tractography/particle filtering/annealing require an enormous number of random samples to provide a reliable solution, being very slow. The present algorithm may run in 90-300 seconds in a 2007' laptop.
- Since the solution is deterministic, the convergence to the theoretically optimal solution is guaranteed.
- Compared to *local* algorithms, the use of global information makes this method quite robust to noise and artifacts.
- This algorithm will always find a connection between the seeds and the targets, even in the presence of very noisy data or extreme artifacts.
- It takes DWI and not DTI as input, so in principle it is not affected by the limitations of the diffusion tensor model (e.g. fiber-crossings handling).
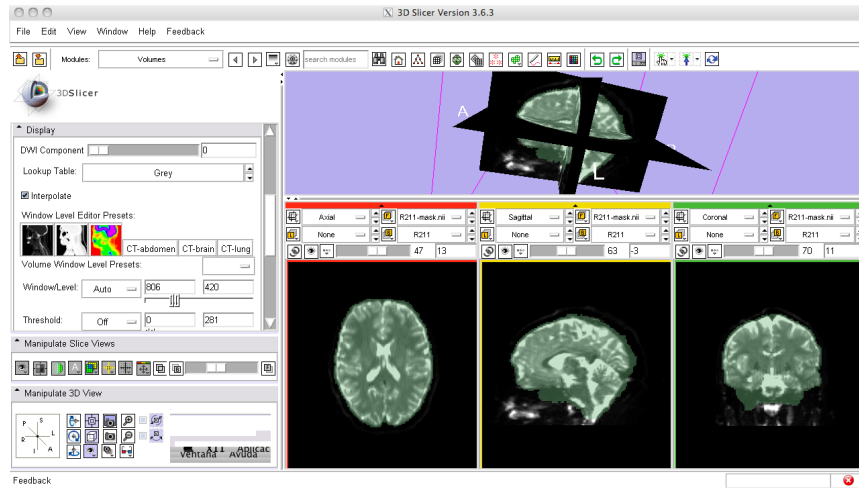
Its main drawbacks are:

Fig. 2. Input HARDI-DWI volume with the ROI superimposed.

– It is still slow compared to standard methods like Runge-Kutta integration.
– Though it can work with regular DTI data, it is intended for HARDI-DWI, which imposes severe constraints in the kind of studies it is suitable for.
– **Since it always finds a connection between seeds and targets, it can find unlikely/incorrect tracts if these regions are wrongly placed.**
– The costs computed do not have an intuitive physical interpretation.
– The segmentation of both seed and target regions implies extra work.

4   Analysis pipeline

The input to the algorithm in all cases is the DWI volume provided. No further filtering/eddy current correction has been done in any case.

1.- We compute a mask (ROI) to remove the background from the computations using 3D Slicer: i) A DTI volume is estimated from the DWI. ii) The FA is computed. iii) The FA map is smoothed with a Gaussian filter with $\sigma = 2$. iv) The map is thresholded. v) The mask obtained is manually edited if needed.

2.- The labels (seed and target regions) are manually segmented using 3D Slicer by an untrained/inexperienced/impatient user. i) The seeds are placed in 3-5 axial slices in the cerebellar peduncle. ii) The targets are placed in several coronal slices using a color-orientation image as a guidance; these slices are chosen approximately in the same vertical as the seeding points, whenever the cingulum is well visible and clearly following the anterior-posterior direction.

3.- i) The program to compute the costs and arrival directions maps is run in each case. ii) The program to back-trace the arrival directions map from the targets to the seeding region is run. No correction of the segmentations is performed regardless of the results of this step.
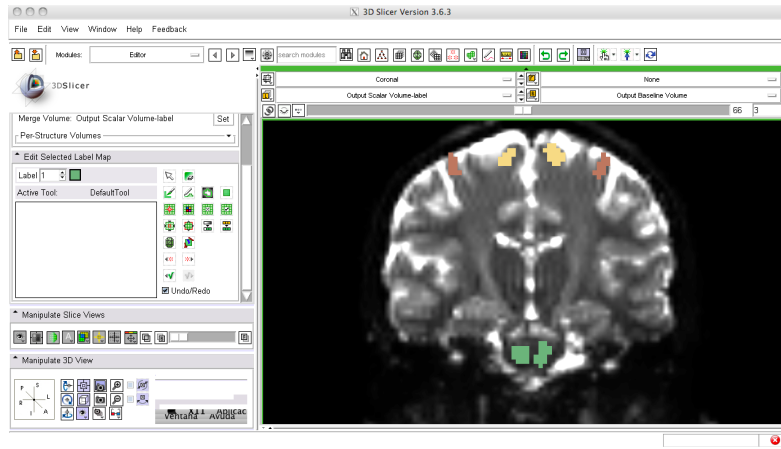
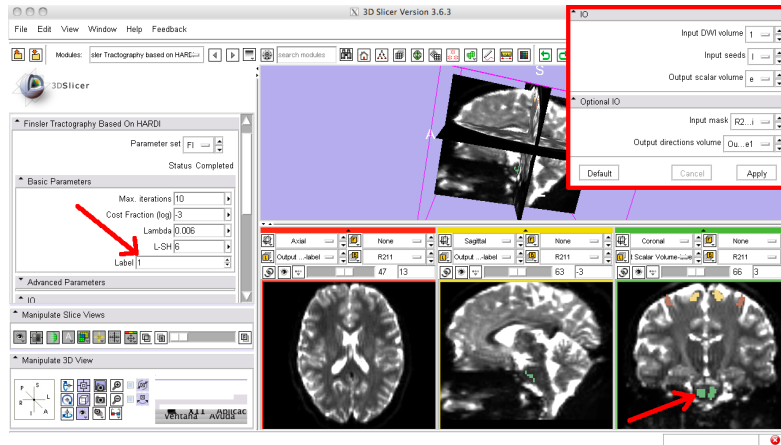**Fig. 3.** Label map of seeding and target regions manually segmented.

Fig. 4. Module to compute the costs and arrival directions maps. The Finsler distance will be computed from the region labeled "1" to the rest of the points in the ROI.

NOTE: For the healthy subjects, we have segmented (mask and label images) only the first scan. The maps are projected to the spaces of the remaining scans using a *home-made* implementation of the *demons* registration algorithm [2]. We use the T2-unweighted baselines of each DWI for reference.

5   Sample images

Figures 2 through 6 present a simple case illustrating the whole processing pipeline for the Finsler fiber-tracking method.
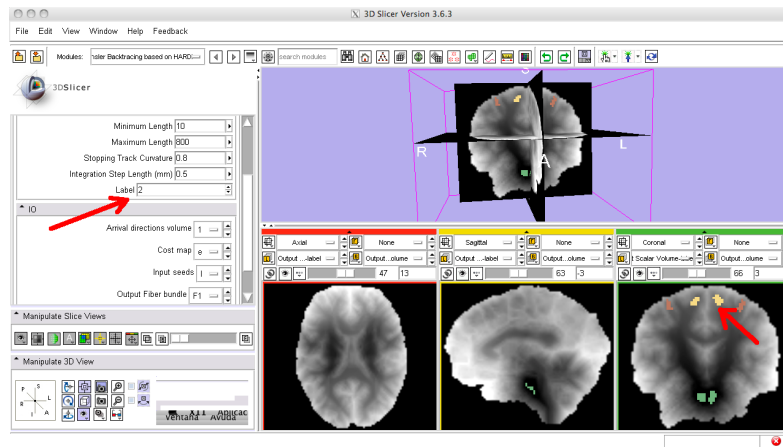
Acknowledments

Fig. 5. Example of costs map. The cost is minimum (zero) in the region labeled "1", since there is no cost to reach this region from itself. For the rest of the volume, regions in the white matter are more easily reached than the others, since they are connected to the seeding region through fiber tracts. In particular, the cost in the region labeled "2" is rather low, and the fiber tracts will be traced back from it to the seeding region.
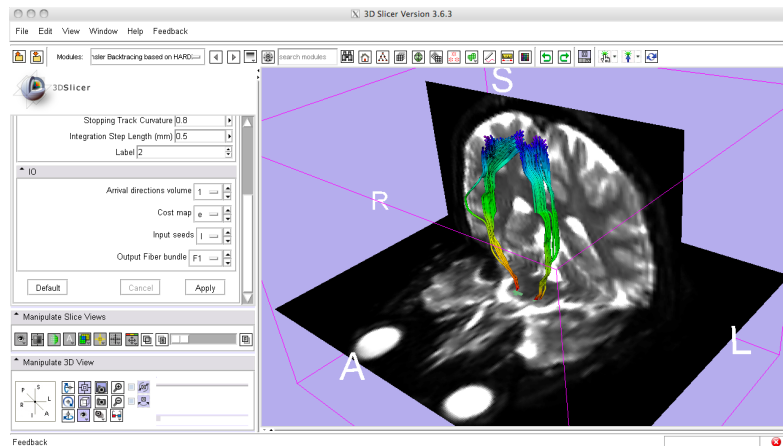

Fig. 6. Reconstruction of the corticospinal tract using the back-tracing module.

References

1. Melonakos, J., Pichon, E., Angenent, S., Tannenbaum, A.: Finsler active contours. IEEE Trans. Pattern Analysis and Machine Intelligence **30**(3) (2008) 412–423
2. Tristán-Vega, A., Vegas-Sánchez-Ferrero, G., Aja-Fernández, S.: Local similarity measures for demons-like registration algorithms. In: Proc. IEEE Int. Sym. Biomed. Im.: From Nano to Macro, Paris, France (2008) 1087–1090

DTI Tractography Challenge-MICCAI 2011: A Volumetric Approach to extract Corticospinal tract in Diffusion Tensor MRI

Gopal B Veni, Xiang Hao, Kristen Zygmunt, P. Thomas Fletcher and Ross T. Whitaker

Scientific Computing and Imaging Institute
University of Utah
Salt Lake City, Utah 84112
{gveni,hao,krismz,fletcher,whitaker}@sci.utah.edu
http://www.sci.utah.edu

1 Introduction

This report presents our volumetric segmentation approach to determine the white matter connectivity, specifically in the corticospinal tract. The complete analysis is based on the work by Fletcher *et al* [1], which uses a Hamilton-Jacobi (H-J) formulation and a fast iterative method to minimize the total path cost between two seed regions. The total cost is defined as the integral of local costs obtained from the tensor information along the path. This leads to a region-to-region connectivity providing a volumetric representation of the white matter pathway between two regions.

2 DTI analysis pipeline

Once the seed regions are defined that represent two target regions of the volumetric pathway, the local cost is calculated at each point on the image using its tensor information. This is followed by a nonlinear partial differential equation which computes minimal cost from the first target region to every point in the image. Similarly, the minimal cost is computed from a second target region. The two solutions are then combined in order to produce a minimum cost path between the two regions.

As [1] quotes, given a path $c : [a, b] \to \Omega$, where Ω is an image domain, the total cost of c is defined as

$$E(c) = \int_a^b \psi(c(t), T(t))dt, \tag{1}$$

where $T(t) = \frac{c'(t)}{\|c'(t)\|}$ is the unit tangent vector of c. The local cost function, $\psi(x, v)$ gives the cost of moving in the unit direction v from point x. Following [2], a quadratic local cost function is used which is defined as

$$\psi(x, v) = v^T M^{-1}(x)v, \tag{2}$$

where $M(x)$ is a symmetric, positive-definite matrix defined at each point $x \in \Omega$.

Instead of directly choosing the tensors in place of M, they are sharpened by raising it to a power α so that the solution tends to follow the white matter pathway rather than the shortest path in the Euclidean sense. Now, if the sharpened tensor is considered to be the speed (in the H-J formulation), which gives low cost along the principal eigen directions, the cost is the inverse. Thus we have

$$M(x) = |D(x)|^{\frac{1}{3}} \left(\frac{D(x)}{|D(x)^{\frac{1}{3}}|}\right)^{\alpha}, \tag{3}$$

where $\alpha > 1$ and $|D(x)|$ denotes the determinant of $D(x)$. Let γ be the optimal path obtained using H-J formulation and ϵ be the tolerance of paths relative to the optimum. A set of all points whose constrained minimum cost is less than $(1 + \epsilon)E(\gamma)$ is defined as a volumetric pathway between the two target regions. Thus the segmented voxels describe the fiber connection between them.

To solve numerically the H-J equation, the Fast Iterative Method [3] is used due to its speed. As our analysis is mainly concerned with the white matter connectivity, a white matter mask is generated to solve for the cost function. For numerical accuracy, the solution on the grid is supersampled by two from the original data.

3   Results

The DTI volumetric segmentation framework has been applied to two healthy and two neurosurgical cases. The analysis was carried out to segment the left and the right corticospinal tracts in datasets. Using the color-coded orientation map that can be calculated using the tensor volume, we outlined the terminal regions manually for these tracks. A DTI atlas by Mori [4] has been used as a guideline to define these seed regions on our colored orientation maps.

Figure 1 illustrates one example of seed regions on a healthy subject. Figure 2 illustrates results that depict the segmented corticospinal tracts on a healthy and neurosurgical case. According to the figure, these segmented regions are overlayed on T-1 weighted MR images as well as colored Eigenvector images. An α value of 3 and an ϵ value of 0.06 are chosen for all cases.

References

1. Fletcher, P.T, Tao, R., Jeong, W, Whitaker, R.T.: A Volumetric approach to Quatifying Region-to-Region white Matter Connectivity in Diffusion Tensor MRI. Proceedings of Information Processing in Medical Imaging (IPMI); (2007) pp. 346-358
2. Pichon, E., Westin, C.F., Tannenbaum, A.: A Hamilton-Jacobi-Bellman approach to high angular resolution diffusion tractography. In: MICCAI. (2005) pp. 180-187
3. Zhao, H.: A fast sweeping method for eikonal equations. Mathematics of Computation 74(2004) pp. 603-627
4. Mori, S., Wakana, S., Nagae-Poetscher, L.M., van Zijl, P.C.M.: MRI Atlas of Human White Matter. 1st Edition, Elsevier (2005), ISBN: 0-444-51741-3
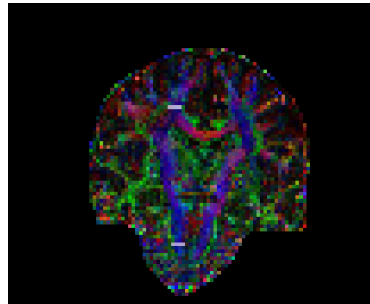
Fig. 1: White regions indicate seeds defined for Corticospinal tract on a healthy case

(a) Neurosurgical View1   (b) Neurosurgical View2

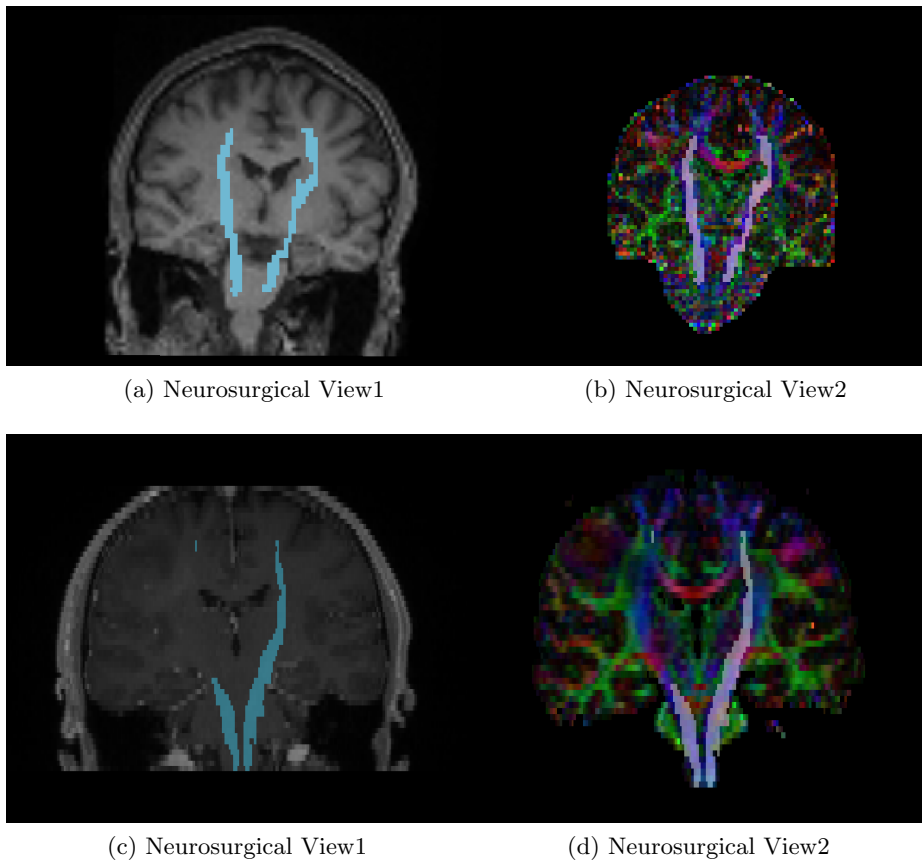(c) Neurosurgical View1   (d) Neurosurgical View2

Fig. 2: (a) DTI volumetric segmentation results on a healthy subject T1-weighted image; (b) DTI volumetric segmentation results on colored eigen-vector image; (c) DTI volumetric segmentation results on a patient T1-weighted image; (d) DTI volumetric segmentation results on colored eigen-vector image